Ph.D. DISSERTATION

Robust Design of Organic Rankine Cycle Using Uncertainty Quantification Method

불확실성 정량화를 이용한 유기랭킨사이클의 강건한 설계에 관한 연구

BY

KIM KYEONGSU

FEBRUARY 2019

DEPARTMENT OF CHEMICAL AND
BIOLOGICAL ENGINEERING
COLLEGE OF ENGINEERING
SEOUL NATIONAL UNIVERSITY

Ph.D. DISSERTATION

Robust Design of Organic Rankine Cycle Using Uncertainty Quantification Method

불확실성 정량화를 이용한 유기랭킨사이클의 강건한 설계에 관한 연구

BY

KIM KYEONGSU

FEBRUARY 2019

DEPARTMENT OF CHEMICAL AND
BIOLOGICAL ENGINEERING
COLLEGE OF ENGINEERING
SEOUL NATIONAL UNIVERSITY

Robust Design of Organic Rankine Cycle Using Uncertainty Quantification Method

불확실성 정량화를 이용한 유기랭킨사이클의 강건한 설계에 관한 연구

지도교수 이 원 보

이 논문을 공학박사 학위논문으로 제출함

2019년 2월

서울대학교 대학원

화학생물공학부

김 경 수

김경수의 공학박사 학위 논문을 인준함

2019년 2월

위 원 장: _____
부위원장: _____
위 원: _____
위 원: _____
위 원: _____

Abstract

A method to design the optimal working fluid mixture of Organic Rankine Cycles (ORC), which is operationally flexible and robust against measurement error in thermodynamic parameters, has been developed. Prior to design robust ORC, an optimal design of ORC for utilizing Liquefied Natural Gas (LNG) as heat sink of which evaporation process is not isothermal is proposed to represent a design procedure to extract as much energy as possible from a multicomponent heat sink without consideration of robustness. The proposed system adopts binary working fluids for each stage to minimize the exergy destroyed in the condensers of each stage of the cycle. The best combination of working fluids was selected through minimization of the amount of destroyed exergy by varying the flow rate, composition, and pressure of the working fluid. After selecting the working fluids, process optimization was performed through a parametric study. In addition, a sensitivity analysis was performed to observe the effect of temperature variation of the heat sources in the range of 25 - 85 °C on the net power generation.

At the following section, a systematic method to design a robust ORC using LNG and multicomponent working fluid, which yields maximum power output even when the composition of the working fluid varies from the nominal point during operation of ORC has been developed. The proposed method seeks the optimal composition giving both the maximum mean of ORC power output. To suppress the factors that

adversely affect the operation of ORC (violation of minimum temperature difference in heat exchanger and formation of liquid droplet in expander), the objective function is penalized when they occur. The procedure to derive the statistical moments consists of two steps. Initially, the required heat exchanger area is obtained by simulation of ORC model with a nominal operating conditions (composition, pump discharge pressure, and expander discharge pressure). At the next step, the simulation is carried out again with the obtained area and the varying composition. The mass fraction of each substance in the working fluid is assumed to follow uniform distribution centered at the nominal point. To obtain the mean and variance with a small number of simulations, Polynomial Chaos Expansion (PCE) with sparse grid quadrature is employed. It has been shown that small changes in composition can have serious consequences for stable operation of ORC, and the design of working fluid by the proposed method allows flexible ORC operation despite the existence of uncertainty in the composition.

Finally, the optimization takes into account uncertainties in thermodynamic parameters and heat source in addition to composition. Using the selected working fluid which was turned out to be the most insensitive from the uncertainty of composition, optimization is carried out again when the critical temperature and pressure of each substance composing the working fluid varies within its measurement uncertainty, which can be found in the literatures. Also, the temperature of the heat source varies from the nominal design point to enhance the operational flexibility of ORC. In sum, the design of ORC was performed assuming a total of the nine parameters or design

variables with uncertainty, which requires excessive amount of computation with the method suggested in the previous section. Therefore, the optimization using a surrogate model was devised to efficiently find the optimal and robust ORC design. Because the proposed surrogate model is constructed based on PCE, the statistical moments can be derived analytically, which leads to reduce the time for optimization drastically. Comparing the ORC design, which was taken with more uncertainty, to the design obtained in the previous section, the former design showed the highest output even when the parameters and design variables were changing from the nominal point.

keywords: Organic Rankine cycle, Robust design, Polynomial chaos, Uncertainty quantification, Multicomponent working fluid

student number: 2013-23159

Contents

List of Tables

List of Figures

Chapter 1

Introduction

1.1 Motivation

Natural gas is one of the most widely used form of fossil fuel with high levels of energy production and low greenhouse gas emissions. For transportation, it is liquefied, and transported to a regasification terminal carrying considerable amounts of energy. This energy is wasted during regasification if no retrieving process is applied. For this reason, various methods have been studied to recover this energy into some form of application at regasification terminals, and organic Rankine cycles (ORCs) have been known to be one of the most effective. In designing ORC using Liquefied Natural Gas (LNG) as heat sink, one common issue is that the sink consists of more than one substance, which diminishes thermal efficiency by increasing the amount of exergy destruction in heat exchangers. Many studies have shown that it is inevitable to use a multicomponent working fluid to achieve high thermal efficiency [1, 2, 3]. This is

because, with optimally selected working fluid substances and composition, it is advantageous in minimizing the exergy destruction in the heat exchanger by fitting the temperature glide of evaporation process or condensation process of working fluid to that of heat source or sink. Some studies were published on the recovery of LNG cold exergy using multicomponent working fluids to extract cold exergy more effectively from LNG [4]. However, no attempt has been made to increase efficiency by combining multicomponent working fluids and multistage process configurations, which can result in further improvement of the thermal efficiency.

Although an ORC design succeeds in significantly improving the efficiency, the working fluid obtained as a result of the optimization methods would not be suitable for an actual ORC because of its vulnerability to uncertainties in operating conditions. Regardless of which criteria are used, the optimization methods design working fluids that can boost the performance of the ORC to the extreme. An ORC using these "optimally designed" working fluid may be in a situation where the net power output decreases severely or its operation becomes infeasible even with a slight change in operation conditions. Therefore, a working fluid and an ORC design which are insensitive to operational conditions should be selected and uncertain factors that impede the stable production of power output at high efficiency should be considered at the design phase.

The uncertainties to be considered in the design phase for a robust ORC can be enumerated numerously, but it is infeasible to design an ORC considering all of them

because of the enormous amount of computation. Therefore, it is necessary to consider only the representative and most influential uncertainties in operation of the ORC, and these can be classified into two categories; the uncertainties that affect the operational flexibility and the uncertainties of thermodynamic parameters due to measurement error. An ORC which was designed considering only the former uncertainties is expected to yield relatively high amount of power when the operating condition varies from its nominal point but still, it can not be sure that the ORC will show efficiency obtained by simulation when it is actually installed. Most of the thermodynamic parameters obtained from experiments are subject to a certain range of uncertainties, which causes the designed process to be unable to have as much performance as expected. Thus, both of the two categories of uncertainties should be considered in the design phase to obtain a robust ORC design.

The stochastic optimization for obtaining robust design usually utilizes statistical moments, which require huge computational effort to obtain. The issue on excessive amount of computation is shared by all stochastic optimization problems, and the same is true for the optimization to obtain robust ORC design. Due to this issue, it is needed to develop a novel design procedure or optimization method to optimize the ORC in reasonable time.

1.2 Thesis outline

In Section 1.3, the standard configuration of ORC is presented. Based on it, Chapter 2 suggests the novel ORC design procedure to maximally draw cold energy from LNG, and the resulting cascade ORC using binary working fluids is presented. In Chapter 3, for ease of discussion, an optimization procedure to design a robust ORC using the basic ORC configuration introduced in Section 1.3. Here, it is assumed that only the composition of working fluid mixture varies during the operation of ORC, and other design variables and parameters are fixed at the nominal point. The reason is that, first of all, rather than dealing with many uncertainties at ones, relatively simple case is discussed and then it will expand to have more consideration on uncertainties. Secondly, the composition has different characteristics from other uncertainties, which is an optimization variable and an uncertain variable at the same time. The details can be found at Chapter 3.

Once the optimization method to design an ORC which is robust against the uncertainty in the composition in Chapter 3, it is properly transformed to deal more uncertainties including the composition, the temperature of heat source, and the thermodynamic parameters. To reduce the required time for the optimization efficiently, construction of a surrogate model is carried out. After demonstrating the design of a robust ORC under 9-dimensional uncertainty variables is feasible using the developed method, the concluding remarks and the future working to improve the proposed method are provided in Chapter 5.

1.3 Conventional ORC configuration

An ORC produces electricity through the expansion process of a pressurized organic working fluid. Since an ORC uses an organic fluid as a working fluid of which boiling point is relatively low, it usually serves to convert low-grade heat to useful power. As illustrated in Fig. 1.1, the conventional ORC consists of four main units; expander, condenser, pump, and evaporator. The working fluid in the condenser discards its heat to the heat sink and is liquefied. Then, the working fluid in the liquid phase becomes pressurized in the pump. In the evaporator, the working fluid receives heat from the heat source and is vaporized. The working fluid in the vapor phase generates power while going through the expansion process in the turbine.

The thermodynamic efficiency of ORC is known to be mainly dependent on exergy destruction in heat exchangers [5, 6]. The exergy destruction, which is equivalent to the loss of available energy occurring when the energy of heat source or heat sink is transferred to the working fluid, can be reduced by adjusting process variables and selecting working fluid alternatives. In particular, when the process that heat source or sink exchanges heat with a working fluid is not isothermal, the effect of well-designed working fluid appears significant. In this case, using a multicomponent fluid instead of a pure fluid as a working fluid has the greatest effect on the reduction of the exergy destruction. Many studies on usage of multicomponent working fluid have reported performance improvement of ORC [7, 8] and also, some studies have shown that the efficiency of ORC using LNG as a heat sink can be drastically improved by adopting

multicomponent working fluids [1, 2, 3].

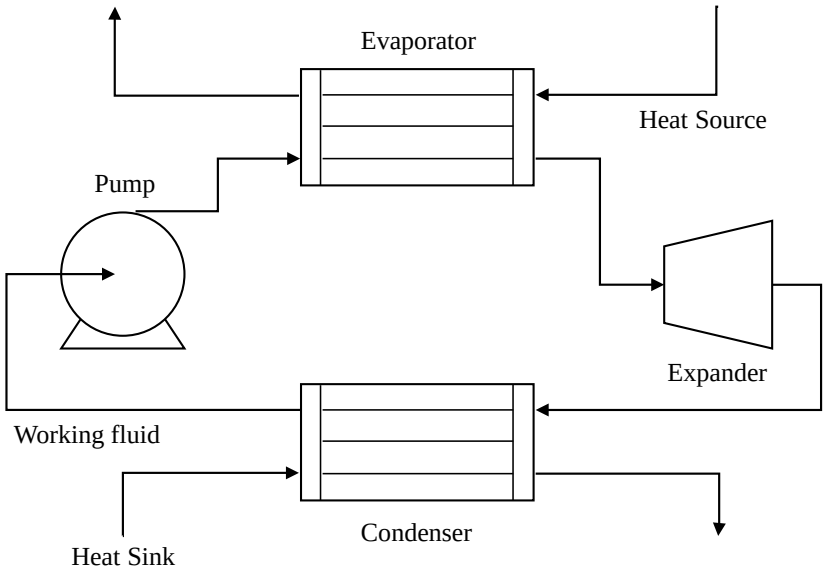

Figure 1.1: Conventional configuration of ORC.

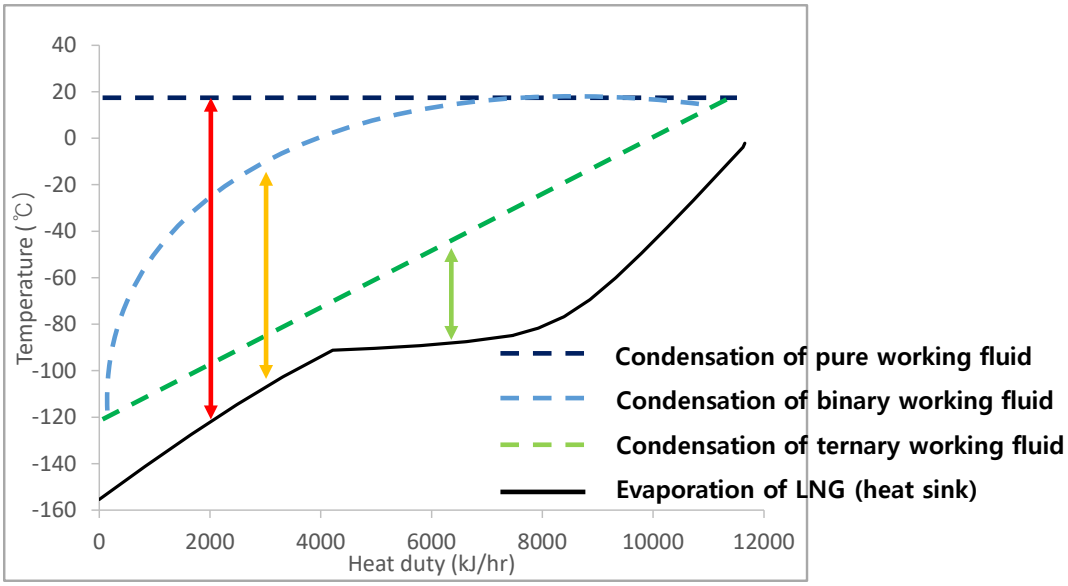

Figure 1.2: Conceptual representation of composite curves in ORC condenser depending on working fluid.

In designing ORC using LNG, the effect of a multicomponent on the reduction of exergy destruction can be seen in Fig. 1.2. The area between heat curves of working fluids and LNG, which represents the exergy destruction increases as the working fluid is composed of fewer substances. The multicomponent working fluid is advantageous to fit the temperature glide of the LNG vaporization process to the working fluid condensation process, so it can reduce the exergy destruction in the condenser. However, more substances do not always lead to higher efficiency, rather it can make designing an ORC more difficult by increasing the number of optimization variables (Adding a substance to a working fluid mixture expands the optimization search space by one dimension because the optimal fraction for the added substance should be found). Previous works on the design of ORC using LNG as heat sink has concluded that a binary or a ternary mixture fluid is the optimal working fluid mixture, and therefore in this study, the design of working fluid using these two type of working fluid will be carried out [1, 2, 3, 4]. More components than ternary mixture should be discussed in future study.

Chapter 2

Design and optimization of cascade organic Rankine cycle for recovering cryogenic energy from liquefied natural gas using binary working fluid

2.1 Background

Many studies have been conducted on the use of LNG (liquefied natural gas) as the heat sink of an ORC, involving analyses of the key parameters and the development of new cycle configurations. Shi and Che proposed a combined power system integrating an LNG power generation cycle with an ammonia-water mixture Rankine cycle [9]. Their study analyzed key variables such as the ammonia turbine inlet pressure,

This chapter was written by reconstructing the previously published paper with the same title. https://doi.org/10.1016/j.energy.2015.05.047

ammonia mass fraction, LNG turbine inlet pressure, and heat source temperature. Liu and Guo proposed a novel cryogenic cycle combined with a vapor absorption process to improve efficiency of the energy recovery rate [3]. Optimization of the key variables resulted in increased efficiency compared to the conventional ORC by 66.3%. Zhang and Lior presented a novel LNG-fueled power plant with a high efficiency and virtually zero CO2 emissions [10]. The proposed cycle was an integrated form of a supercritical CO2 Rankine-like cycle and a CO2 Brayton cycle, with a recuperation system to connect the two. Wang et al. analyzed the thermodynamic aspects of an ammonia-water-based power system with an LNG heat sink [11]. Optimization of the three main objective functions, the exergy efficiency, total heat transfer capability, and turbine size was performed to find the exergy efficiency. Gomez et al. also performed a thermodynamic analysis of the combined cycle of a closed Brayton cycle and a steam Rankine cycle [12]. Choi et al. performed an optimization of a cascade ORC system utilizing the cold exergy of LNG [13]. They concluded that a three-stage cascade ORC using a propane working fluid produced the most electricity. Lee et al. introduced an ORC using LNG to a stream cycle with the CO2 capture process [14]. The amount of power generated was increased by 73% compared to the conventional case, and the energy requirement for CO2 liquefaction in the CO2 capture process was decreased by 9%. Sun et al. proposed a novel ORC design for the recovery of LNG cold exergy using a ternary mixture working fluid [4]. A working fluid composed of methane, ethane, and propane was selected as the optimum mixture. The proposed cycle produced 1.023

kWh of power without LNG expansion when LNG at 12 bar was used.

Meanwhile, various issues can be considered to maximize the efficiency of the ORC. Selecting the appropriate working fluids is one of the most relevant issues. Previous works have suggested various working fluids in order to elevate the cycle efficiency, including ternary organic mixtures [1], and zeotropic mixtures [15]. Also, many studies have been made to evaluate the performance of different working fluids by applying different modeling and optimization techniques [16, 17, 18, 19, 20, 21, 22, 23, 24, 25, 26, 27, 28, 29]. They applied the selected working fluids to different ORC systems and reported cycle efficiency increase from 15 [15] to 56% [1], compared to the conventional working fluids.

Another important issue in ORC cycle research is the design of a novel Rankine cycle configuration. Xu et al. created a regenerator-integrated ORC (RORC), using a vapor injector as the regenerator [30]. Using R123 as the working fluid, a performance comparison was done between the RORC and conventional ORC, where RORC showed better thermal performance. Lemort et al. modeled and tested a scroll expander-integrated ORC [31]. Using HCFC-123 as the refrigerant, they sorted out the important variables, and the model showed a close match with the actual measurements. Zamfirescu et al. studied the performance of an ORC using a positive displacement expander to flash the saturated liquid [32]. Other various studies have been conducted on increasing the efficiency of different ORC configurations [33, 34], and the use of various modeling techniques [35].

Different heat sources result in different power outputs, and many studies have been conducted on the use of available heat sources. These include geothermal energy [21, 28] and solar energy [19, 25].

Recently, some studies were published on the recovery of LNG cold exergy using multi-component working fluids to extract cold exergy more effectively from LNG [3, 4]. However, the efficiency needs to be further improved. In this study, a novel cascade Rankine cycle design using binary mixture working fluids to utilize LNG cryogenic energy was proposed for enhancing the efficiency of LNG regasification terminals. Both the configuration and the binary working fluid selection contributes to the objective of maximizing the power output. LNG cold exergy is thoroughly utilized by a two stage sequential contact with different binary mixture working fluids. An additional stage is synthesized to recover cold exergy that was transferred from LNG to the working fluids of the first two stages, conducting a three-stage configuration. A total of three stages were optimized in a sequential manner, considering the relevant variables selected by a parametric study.

2.2 Description of the proposed cascade organic Rankine cycle

To reduce some confusions, the cycle indicates the whole power generation system and the stage indicates each stage which composes the whole cycle. A new concept for a cascade ORC was proposed in this study. Three stages were used, and each stage used a binary mixture as the working fluid. The basic concept of the proposed system can be summarized as Fig. 2.1. The first stage and the second stage are in a series arrangement to recover the cold exergy of LNG more efficiently. The working fluids of the first stage and the second stage receive the cold exergy from LNG directly. Thus, the first and second stages are considered as a process block called LNG cold exergy recovery part. The first stage can recover only a part of LNG cold exergy in lower temperature level so some amount of LNG cold exergy remains to be utilized at relatively higher temperature level. Then, the second stage recovers the remaining cold exergy of LNG. Each stage adopts a binary working fluid in order to reduce the irreversibility. Recovering the cold exergy throughout two stages in series and adopting binary working fluids make it possible to reduce the irreversibility significantly because it makes the temperature profile of working fluid condensation process fitted to that of LNG regasification process.

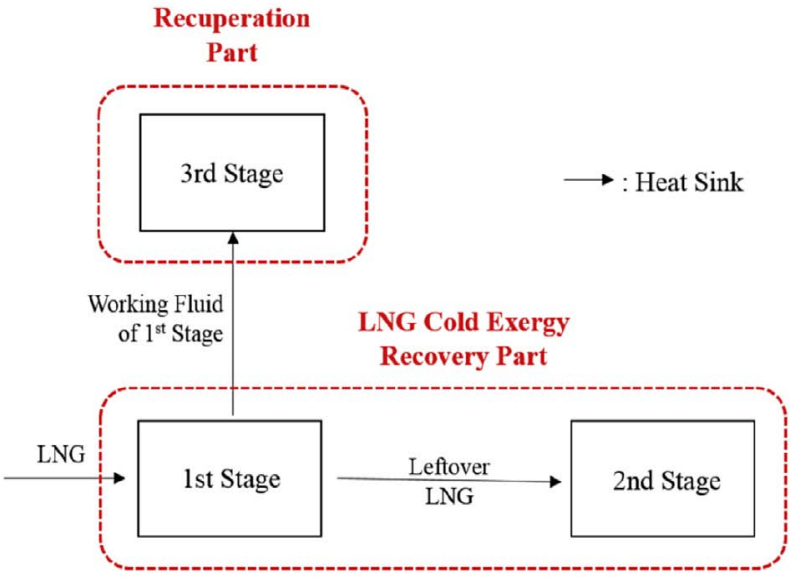

Figure 2.1: Concept for proposed cycle.

Meanwhile, the third stage is parallel with the first stage. The third stage can be considered as a separate process block because it recovers the cold exergy not from the LNG but from the first-stage working fluid. The third stage recuperates the cold exergy from the first stage so this process block is called the recuperation part. There have been studies on ORCs with an LNG heat sink that used a multi-channel exchanger for recovering the cold exergy of the working fluid [13, 4]. However, since the working fluid is designed to fit the temperature gliding of the LNG rather than the working fluid itself, the introduction of a multi-heat exchanger to the cycle can increase the exergy destruction. By introducing a third stage, an appropriate working fluid can be selected to minimize the amount of exergy destroyed when the cold exergy of the first stage is recuperated in the third stage. The third stage also utilizes a binary working fluid to fit the temperature gliding of the first-stage working fluid condensation.

A schematic diagram is presented in Fig. 2.2. To enhance the readability, each component in the schematic diagram is named according to a specific naming system. The name of component is in order of the type of unit, the number of the stage, and a specific number of the component. For instance, the name S1-1 represents that this unit is a stream in the first stage.

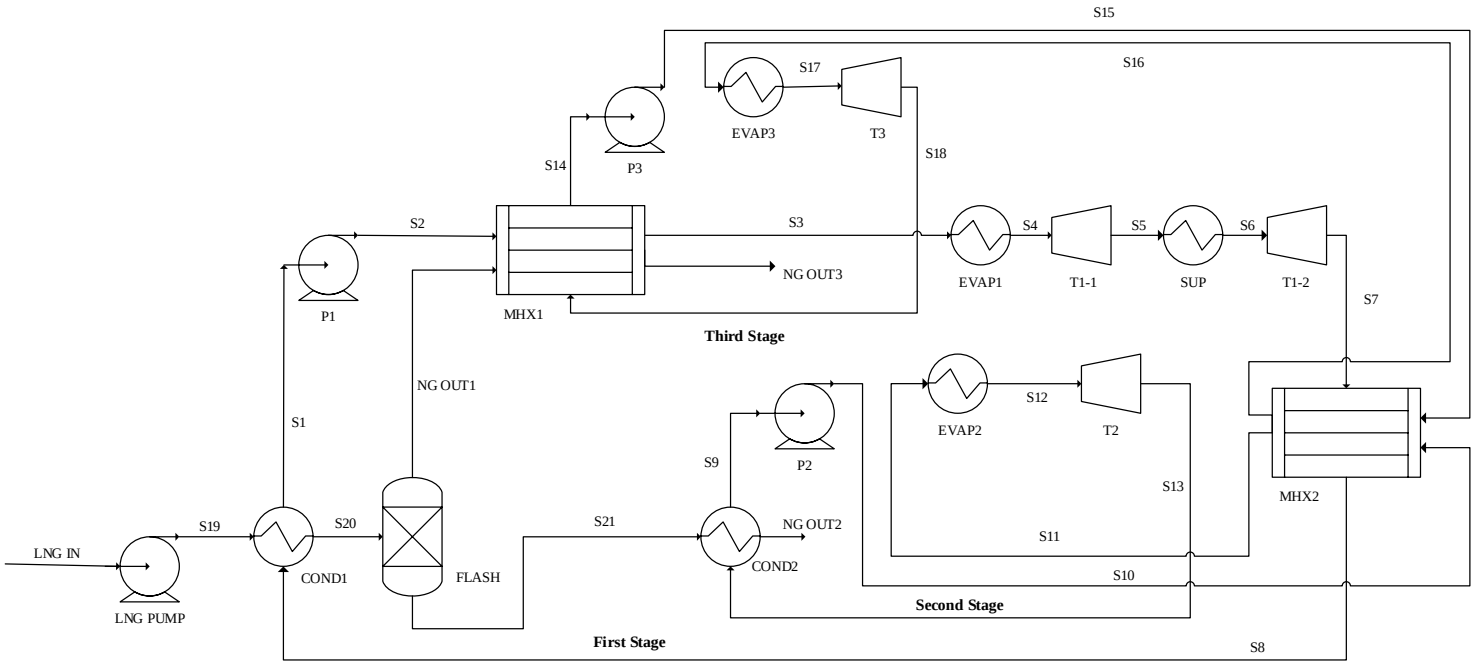

Figure 2.2: Process flow diagram of proposed cascade power generation system.

Table 2.1: Composition of LNG

Component	Mole fraction
N_2	0.0007
Methane	0.8877
Ethane	0.0754
Propane	0.0259
n-butane	0.0056
i-butane	0.0045
n-pentane	0.0001
i-pentane	0.0001

First, the LNG, which has components as summarized in Table 3.2, is pressurized up to 30 bar at the LNG pump and vaporized once at the first-stage condenser (COND 1-1). Then, the rest of the LNG is vaporized at the second-stage condenser (COND 2-1).

Pressurized stream S1-2 is evaporated partially in the multi-channel exchanger (MHX2-1), and part of S1-2 is evaporated MHX2-1. Then, the rest of S1-3 in the liquid phase is evaporated and superheated in evaporator HX 1-1. The superheated working fluid in S1-4 generates power in the first turbine (TURB 1-1) by going through the expansion process until no liquid droplets are produced. The saturated stream S1-5 is superheated again in the superheater (HX 1-2) and expanded in turbine TURB 1e2 to obtain additional power output. Then, stream S1-7 from TRUB 1-2 flows into the multi-heat exchanger MHX 1-1. Stream S1-7 remains in a superheated state as a result of the two-stage expansion process so it should be cooled down to a saturated phase in order to complete the cycle. In MHX 1-1, S1-7 discards heat to S2-2 and S3-2. Finally, S1-8 from MXH 1-1 enters condenser COND 1-1 to be liquefied.

The working fluid of the second stage S2-2 is evaporated partially in the multi-heat exchanger MHX 1-1, and the rest in the liquid phase is evaporated and superheated in evaporator HX 2-1. Other units in the second stage are the same as a basic ORC. The design of the third stage is similar to that of the second stage except for the condenser. In the third stage, the multi-heat exchanger is adopted in place of a condenser because it recovers the cold exergy not only from the first-stage working fluid but also from

NG which is produced at the first-stage condenser COND 1-1.

All the evaporators and superheaters except for the multi-heat exchangers (HX 1-1, HX 1-2, HX 2-1 and HX 2-2) are assumed to use free heat source such as sea water at 25 °C and use different working fluids with each other which is selected via optimization.

2.3 Simulation and optimization of power generation cycle

To simulate the proposed cycle, it was modeled using the commercial process simulator ASPEN PLUS and the optimization was performed through MATLAB. The simulation and optimization were performed in consecutive order as it is presented in Fig. 2.3. At first, the working fluid of the first stage was selected by minimizing the amount of exergy destroyed within the first-stage condenser. The second-stage working fluid is selected afterward, in the same way. Since the second stage utilizes the remaining cold exergy of LNG, the working fluid selection should be performed after the flow rate and the temperature of LNG which flows into the second stage are decided. By combining the results of exergy destruction in the first- and second-stage condensers, the working fluids were chosen to minimize the overall amount of destroyed exergy occurring from heat exchange between the working fluid and LNG. Then, process optimizations of the first and second stages were carried out to obtain maximum power output. Since the third stage is supposed to recover the cold exergy from the first-stage working fluid, the simulation and optimization should be performed after the conditions of the first stage is fixed. Thus, the working fluid selection of the third stage was carried out after the process optimization of the first stage had been completed. At last, the process optimization of the third stage was performed to find the optimal condition of the whole cycle. Throughout the whole cycle, the minimum temperature approach was set at 5 °C. The thermodynamic properties were calculated using the Peng-Robinson equation of state [36], and the ambient temperature T_0 was assumed to be 300 K.

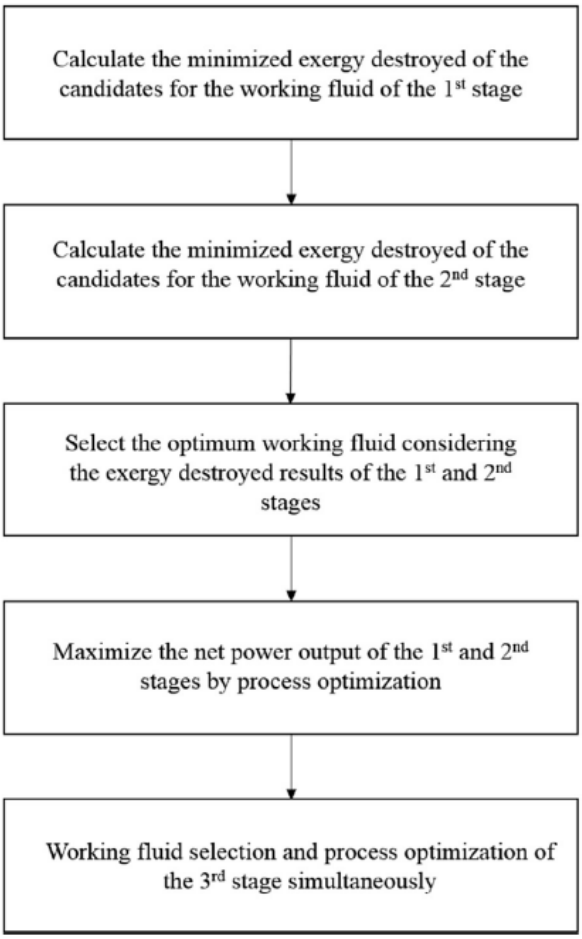

Figure 2.3: Flow chart of optimization.

Table 2.2: Working fluid candidates for each stage.

Stage	Working fluid candidate
First stage	(R14, ethane), (R14, propane), (R14, n-butane), (R14, i-butane), (methane, n-butane), (methane, i-butane), (methane, n-pentane)
Second stage	(ethane, n-butane), (ethane, i-butane), (ethane, n-pentane), (propane, n-pentane)
Third stage	(ethane, n-butane), (ethane, i-butane), (ethane, n-pentane), (propane, n-pentane)

Since each stage has a different operating temperature, the suitable substances for the working fluid candidates vary. A total of six candidates were selected taking into account the temperature ranges of each stage. The candidate binary mixtures for the working fluids are listed in Table 3.6.

2.3.1 LNG cold exergy recovery part

Working fluid selection

The exergy destruction in a condenser was defined as the exergy difference between the cold and hot media.

$$\Delta\bar{e} = \bar{e}_{in} - \bar{e}_{out} = (\bar{h}_{in} - \bar{h}_{out}) - T_0(\bar{s}_{in} - \bar{s}_{out}) \quad (2.1)$$

$$\dot{I}_{cond} = \sum \dot{n}_{hot}\Delta\bar{e}_{hot} + \sum \dot{n}_{cold}\Delta\bar{e}_{cold} \quad (2.2)$$

The amount of exergy destruction in a condenser ($\dot{I}_{cond}$) in Eq. (3.17) depends on the similarity between the temperature gliding behaviors of the LNG and working fluid. Because the physical properties of LNG are fixed, the amount of destroyed exergy is determined by the flow rate, composition, and pressure of the working fluid. Thus, the optimization of each stage condenser was performed by Eqs. (2.3) - (2.6).

$$\text{minimize} \quad \dot{I}_{cond} = F(\dot{n}_{wf}, x_1, P_{wf}) \quad (2.3)$$

$$\text{subject to} \quad \Delta T_{min} \geq 5^{\circ}\text{C} \quad (2.4)$$

$$x_1 + x_2 = 1 \quad (2.5)$$

$$x_1, x_2 \geq , \dot{n}_{wf}, P_{wf} > 0 \quad (2.6)$$

where F is the function of destroyed exergy amount, and x_1 and x_2 are the mole fractions of the two components in the working fluid. $\dot{n}_{wf}$ and P_{wf} are the mole flow rate and pressure of the working fluid, respectively.

The three variables (flow rate, composition, and pressure of the working fluid) determine, not only the exergy destructions in the condensers, but also the amount of

heat exchanged. Since the first stage and the second stage recover the cold exergy of LNG in sequential order, the optimization of the first-stage condenser determines the amount of cold exergy that should be recovered by the second-stage condenser.

Process simulation

All the evaporators and superheaters used a low-grade heat source with a temperature of 25 °C. From the simulation using ASPEN PLUS™, the heat injected to the cycle was calculated by a simple heat balance to analyze the exergy efficiency.

Similarly, the power generated from each turbine and the work used by pump were calculated from the simulator, assuming the isentropic efficiency to be 0.72. To analyze the amount of work produced per unit mass of LNG, the power ($\dot{W}_{tur,i}$) was modified to $W_{tur,i}$ as in Eq. (2.7).

$$W_{tur,i} = \frac{\dot{W}_{tur,i}}{\dot{n}_{LNG} M_{LNG}} \tag{2.7}$$

All the equations for calculating power output were turned into the amount of work using kilogram LNG measure since it makes fair analysis possible when it comes to studying utilization of LNG as many studies pointed out.

To perform a thermal and exergy analysis of the power generation cycle, the total net amount of work should be defined in advance.

$$W_{net} = \sum_i W_{tur,i} - \sum_i W_{pump,i} \tag{2.8}$$

When calculating the efficiency of each stage, all of the streams, including the recuperated exergy flow are considered to compare their efficiencies with those of other

stages. However, when calculating the efficiency of the whole cycle, other streams are excluded, except for the LNG exergy and the heat transferred from the heat sources, because it is appropriate to consider only the exergy transferred from the outer system to the cycle in the evaluation. The cold exergy efficiencies of each stage and the whole cycle are defined as Eq. (2.9) and Eq. (2.10), respectively.

$$\eta_{c,i} = \frac{W_{net,i}}{\sum(e_{in} - e_{out})_{cold}} \tag{2.9}$$

$$\eta_{c} = \frac{W_{net}}{e_{LNG} - e_{NG}} \tag{2.10}$$

Although analyses of the heat sources were excluded, the thermal efficiency η_{th} was calculated to obtain more information.

$$\eta_{th,i} = \frac{n_{LNG}\bar{W}_{net,i}}{Q_{source,i} + Q_{regenerated}} \tag{2.11}$$

$$\eta_{th} = \frac{n_{LNG}\bar{W}_{net}}{\sum_i Q_{source,i}} \tag{2.12}$$

In addition, the overall exergy efficiency was calculated to obtain insight into the proposed cycle.

$$\eta_{ex} = \frac{n_{LNG}\bar{W}_{net}}{n_{LNG}(\bar{e}_{LNG} - \bar{e}_{NG}) + \sum_i Q_{source,i}(1 - \frac{T_{out,i}}{T_{in,i}})} \tag{2.13}$$

Process optimization

The objective of optimization was to maximize the net power produced. Once the properties of the working fluids were determined under the optimum conditions, the whole process optimization was performed. Except for the temperature of heat source which was assumed to be fixed, the pressure of outlet stream from each pump and

the intermediate pressure between two stage turbines which are in the first stage were selected as relevant variables because there was no other option that could be varied on the characteristic of power generation cycle. However, as pointed out on many studies, it is obvious that the exhaust stream should be in saturated phase to obtain largest amount of power output in case of a system using the wet working fluids [1, 8]. Thus the intermediate pressure was lowered as far as possible until the exhaust stream from the first turbine stayed in saturated phase.

The pressure of outlet stream from each pump was decided via a parametric study. The tendency of power output was investigated depending on the pump pressure and the optimum pressure was chosen at the point of largest power output.

Since a sensitivity analysis for cases with different heat sources (25 °C, 45 °C, 65 °C and 85 °C), which covered heat sources in the low-temperature range to the lower part of the medium temperature range [13], was performed, the optimization was carried out for each case.

2.3.2 Recuperation part

Most of the simulation and optimization method for the recuperation part is the same as the LNG exergy recovery part. However, unlike the LNG exergy recovery part, the objective was to provide, not only the minimum exergy destruction, but also the maximum power output, because the third stage did not have any criteria in relation to how much cold exergy of the heat sink should be recovered. In the case of the first and second stages, the full recovery of the LNG regasification process latent heat was the criterion. However, the cold exergy of the condensed first-stage working fluid can be recovered without any limitations as long as the evaporation temperature of the third-stage working fluid is lower than the temperature of the heat source. A greater flow rate for the working fluid made it possible to obtain a greater power output, but it also increased the fraction of the heavy component and the pressure of the working fluid for fitting the temperature gliding in the condenser of the third stage. This is because the temperature of the first-stage working fluid, which is the heat sink in the third stage, increased as the heat duty in the condenser increased. Consequently, the evaporation of the working fluid became more difficult under low-grade heat sources, and this phenomenon reduced the power generation in the third stage. This implies that the minimization of destroyed exergy via working fluid selection does not guarantee the maximum power output. Therefore, the maximization of the power output through the process optimization had to be considered with the minimization of exergy destruction in the third-stage condenser for working fluid selection.

The determination of the working fluid was performed using Eqs. (2.3) - (2.6), and the power output was recorded while varying the composition and the flow rate simultaneously. When the amount of work had the maximum value, the composition and flow rate were determined, that is, the fraction, flow rate, pressure of working fluid, and discharge pressure from the pump were simultaneously considered.

2.4 Simulation and optimization results

2.4.1 Result for LNG cold exergy recovery part

Working fluid selection result

The dependence of the exergy destruction on the heat duty in the first-stage condenser is represented in Fig. 2.4. Among the four combinations containing R14 that were tested for the first stage, the combination of R14-propane clearly showed the minimum amount of exergy destroyed through the entire heat duty range. Thus, it was deemed the most suitable working fluid for the low-temperature part 30 bar LNG cold exergy recovery. Meanwhile, combinations that contained methane were found to be inappropriate working fluids for the 30 bar LNG because the amount of exergy destroyed of all the methane combinations were larger than that of the R14-propane combination. The exergy destruction trend of three methane-based combinations were similar to each other. Thus, making a binary condition using methane did not work out well. Therefore, all the methane combinations were eliminated from the working fluid candidates.

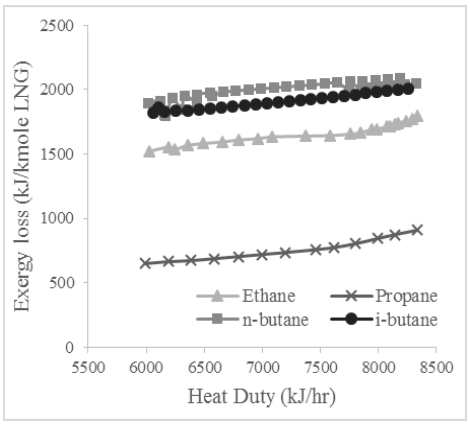

(a) R14 contained

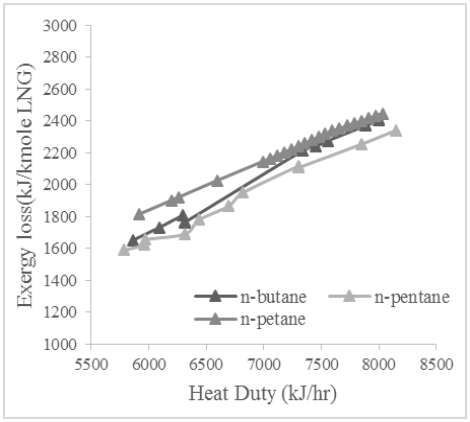

(b) Methane contained

Figure 2.4: Exergy destroyed in first-stage condenser.

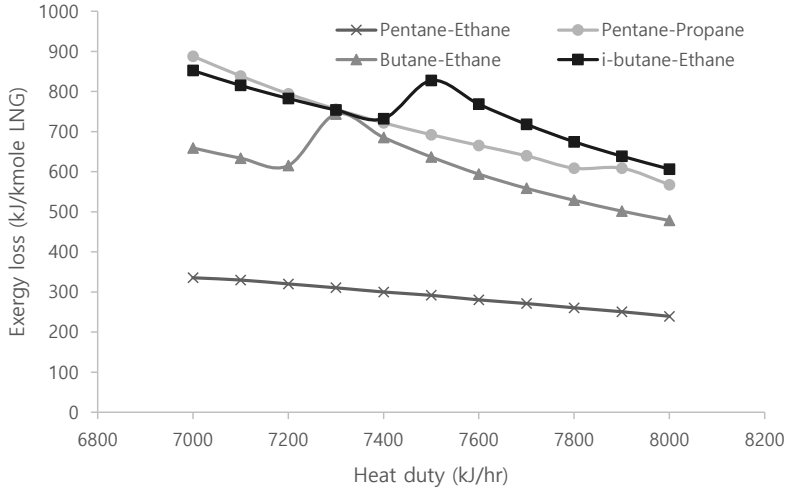

Figure 2.5: Exergy destroyed in second-stage condenser.

In addition, the working fluid selection for the second stage was performed. Fig. 2.5 shows the amount of exergy destroyed in the second-stage condenser according to the heat duty in the first stage condenser. Just as with the results for the first stage, one combination of two pure substances showed a much lower amount of exergy destroyed than those of the other combinations. The optimum combination selected here was an ethane-n-pentane binary mixture, which meant this combination was the most suitable working fluid for the high-temperature part with the 30 bar LNG cold exergy. It can be noticed that some profiles that show local maximum on Fig. 2.5. This is due to the shape of LNG evaporation curve which shows drastic change at some points as in Fig. 11. The nonlinear behavior of the evaporation curve of LNG made pinch points depending on how much of cold exergy had been recovered by the first-stage working fluid.

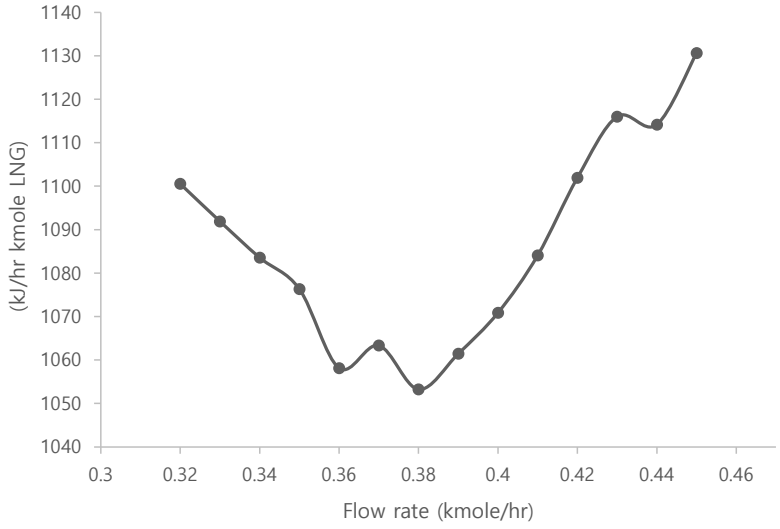

Figure 2.6: Exergy destroyed in second-stage condenser.

Utilizing these two results, which showed that the R14-propane mixture working fluid was the best fit for the first stage and ethane-n-pentane were the best fit for the second stage, the minimum exergy destruction and optimum composition were calculated as illustrated in Fig. 2.6. The sum of exergy destruction amount in the condensers at the LNG cold exergy recovery part (the first and second stage) is plotted in relation to the flow rate of the first-stage working fluid in Fig. 2.6. As it can be seen at Fig. 2.6, the lowest exergy destruction was achieved under a condition where the flow rate of the first stage working fluids was 0.38 kmol/h. At this point, the flow rate of the second stage working fluid was 0.182 kmol/h. In addition, the optimum compositions for the first stage was a 1:1.42 ratio of R14:propane and a 3.26:1 ratio of ethane : n-pentane in the second stage in mole fractions. The details, including the compositions and pressures, are listed in Table 3.

Table 2.3: Working fluid candidates for each stage.

Stage	T of heat source	Combination	Composition (mole fraction)	Flow rate (kmole/h)	Pressure (bar)
First	-	R14 : propane	1 : 1.42	0.38	0.28
Second	-	Ethane : n-pentane	3.26 : 1	0.182	1.71
Third	25	Ethane : n-pentane	0.6 : 1	0.189	0.1
	45		0.9 : 1	0.201	0.2
	65		1.3 : 1	0.23	0.4
	85		1.6 : 1	0.239	0.5

Process simulation and optimization result

A parametric optimization of the first stage was performed, and the result is illustrated in Fig. 2.7. The net power output had an optimal point depending on the discharge pressure from the pump.

The same optimization process was also applied to the second stage. The power output depending on the discharge pressure from the pump in the second stage is shown in Fig. 2.8. Unlike the results for the first stage, the power output increased monotonically as the pressure discharge from the pump increased. This was because the working fluid in the second stage contained a heavier component than that of the first-stage working fluid, which made it hard to evaporate the second-stage working fluid under relatively low temperatures. Consequently, under the condition of higher pressure, the working fluid could not be fully evaporated, and the optimum point was in an infeasible region.

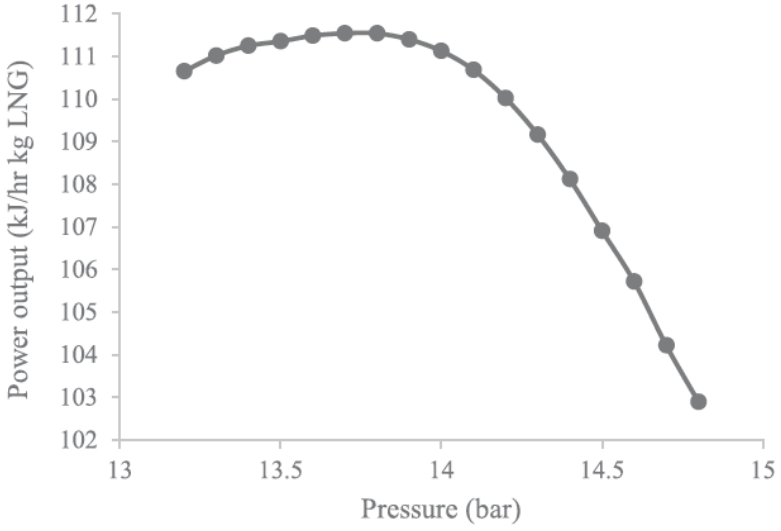

Figure 2.7: Power output of first stage.

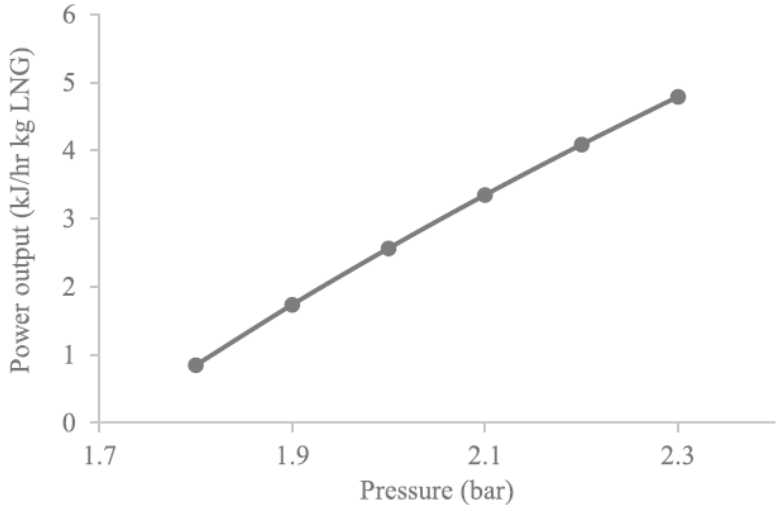

Figure 2.8: Power output of second stage.

2.5 Working fluid selection and process optimization result for recuperation part

Before the working fluid selection for the recuperation part, the process optimization of the first stage was carried out. Using these results, the optimum combination was determined for the third stage. The exergy destroyed in the third-stage condenser are illustrated in Fig. 9. The ethane-n-pentane combination had the lowest exergy destroyed through the entire range. Therefore, the ethane-n-pentane combination was chosen as the optimum. The composition and pressure of this optimum combination were optimized to obtain the maximum power output. The properties of the selected working fluid are listed in Table 3, and the optimization result is listed in Table 4.

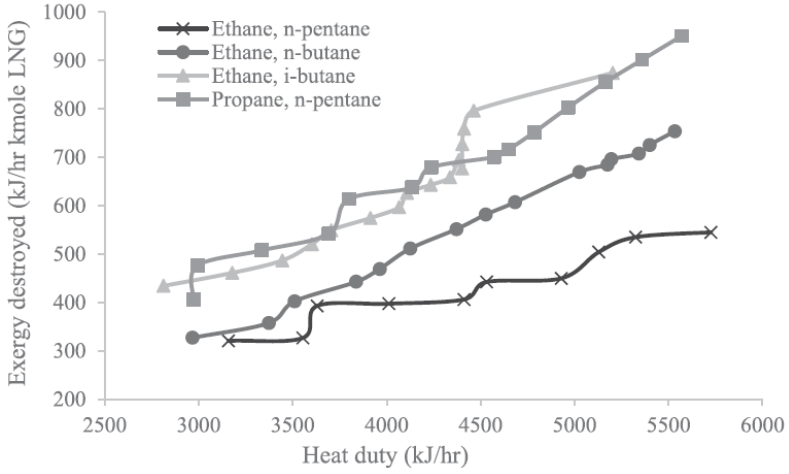

Figure 2.9: Exergy destruction in third-stage multi-heat exchanger.

Table 2.4: Summary of process optimization results for each stage and heat source.

Stage	T of heat source	Pump discharge P (bar)	Power required by pump (kJ/h kgLNG)	Power generated (kJ/h kgLNG)	Net power output (kJ/h kgLNG)	Thermal efficiency (%)	Cold exergy efficiency (%)	Exergy efficiency (%)
First	25	13.7	5.61	117.16	111.54	15.92	22.38	
	45	23.1	9.54	137.06	127.51	17.13	25.21	
	65	35.7	14.81	154.98	140.17	17.74	28.81	
	85	52.7	21.91	171.94	150.03	18.32	29.46	
Second	25	2.3	0.13	4.93	4.8	2.19	3.83	
	45	4.6	0.66	16.66	16	6.96	12.78	
	65	8.9	1.63	27.93	26.3	11	21.00	
	85	15.9	3.22	37.78	34.56	13	27.60	
Third	25	0.9	0.23	35.67	35.44	9.45	18.19	
	45	2.2	0.59	43.74	43.15	11.3	25.53	
	65	5	1.44	53.61	52.17	12.58	30.95	
	85	10.1	3.05	67.25	64.2	14.99	39.25	
Total	25		5.97	157.76	151.78	16.60	21.85	18.64
	45		10.79	197.46	186.66	19.38	22.26	22.26
	65		17.88	236.52	218.64	21.55	24.9	24.9
	85		28.18	276.97	248.79	23.8	27.11	27.11

2.6 Energy and exergy analyses

The cold exergy efficiency was calculated for each stage. As illustrated in Fig. 2.10, which shows the case with the 25 °C heat source, the cold exergy efficiency of the first stage was much higher than that of the second stage. This was because the higher temperature of the heat sink, which reduced the temperature difference between the heat sink and heat source, led to a low power generation. In addition to the temperature of the heat sink, exergy destruction in the condenser can be a cause of the low efficiency. The composite curves of the recovery of the LNG cold exergy part are plotted in Fig. 2.11. The disconnection of the working fluid condensation line at the point where the heat duty is 7461.33 kJ/h occurs because the cold exergy is recovered by two different working fluids. The disconnected point is simultaneously the end point of the first-stage condensation and the start point of the second-stage condensation. It can be readily seen that the temperature difference between the working fluid and LNG in the second-stage condenser is larger than that in the first-stage condenser, which means the working fluid of the second stage recovered the cold exergy less effectively. This can cause lower power generation. As can be seen in Fig. 2.10, most of the LNG cold exergy use takes place in the condenser of the first stage. It is a strong point in favor of a cascade system that the best efficiency appears at the stage where the largest cold exergy is consumed. In this way, the proposed cascade organic Rankine cycle utilizes the limited cold exergy of LNG by effectively minimizing the amount of destroyed exergy.

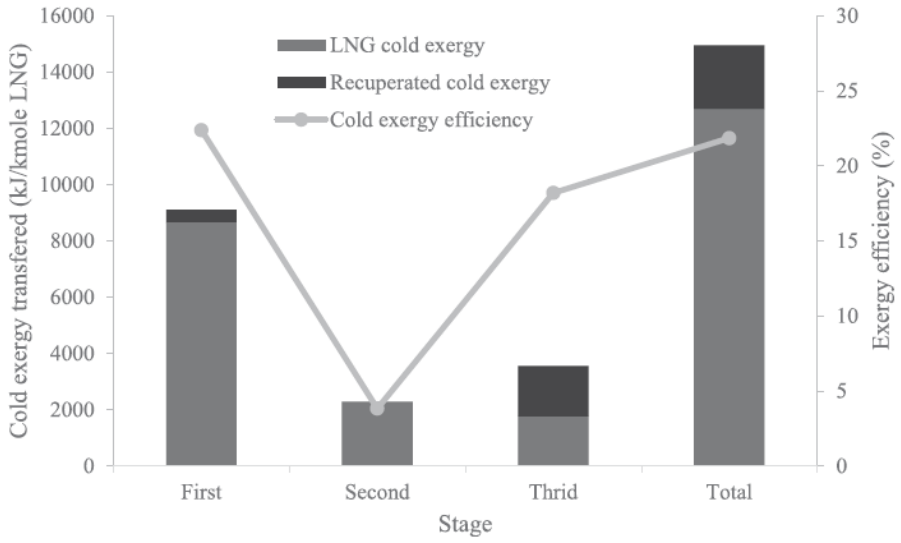

Figure 2.10: Cold exergy input and cold exergy efficiency.

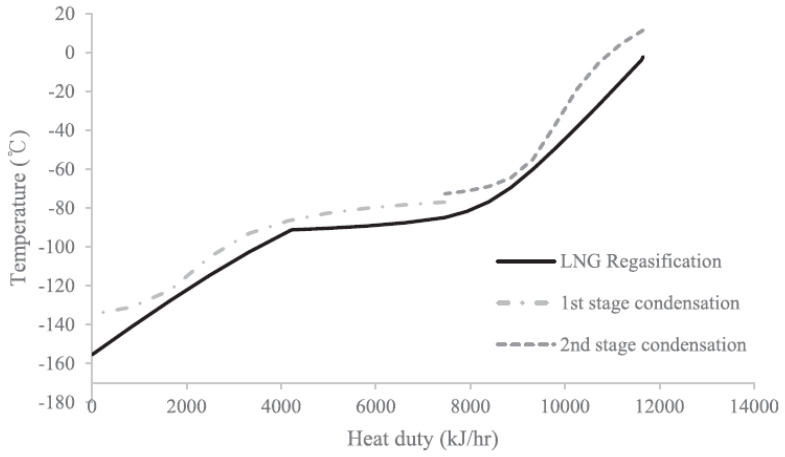

Figure 2.11: Composite curves of first- and second-stage condensers.

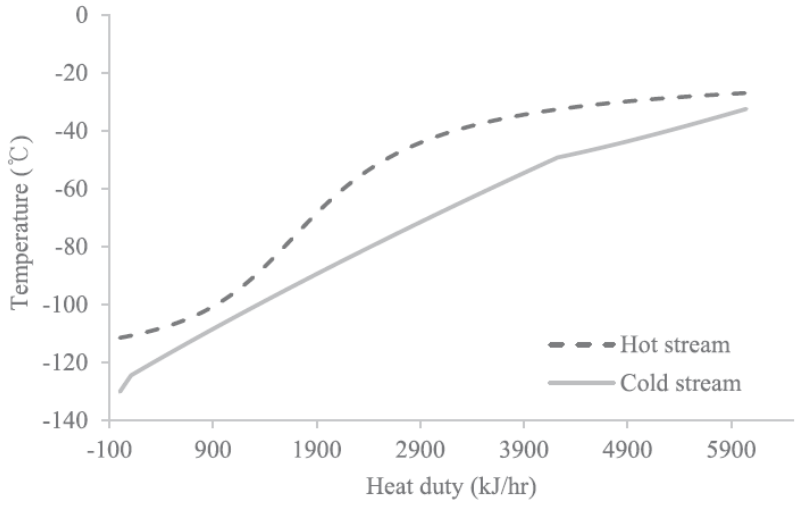

Figure 2.12: Composite curves of third-stage condenser.

In addition, Fig. 2.10 shows the cold exergy efficiency of the third stage and LNG cold exergy used in the third stage. The cold exergy used seems smaller than that of the second stage, but the total cold exergy utilized is the result of the addition of recuperated exergy. Meanwhile, the cold exergy efficiency of the third stage is relatively high. It can be seen that the composite curves of the hot and cold streams fit together, which indicates the minimization of the waste exergy. This can be checked using the composite curves plotted in Fig. 2.12. Consequently, the proposed cycle shows a high efficiency in the place where a large amount of cold exergy is consumed, which indicates the efficient use of the limited cold exergy.

The third stage produces more electricity than the second stage. This can be explained by the sources of cold exergy. The third stage utilizes the sensible heat of NG, as well as part of the latent heat from the first-stage working fluid evaporation. Thus, the third stage is given more cryogenic exergy than the second stage, which leads to the generation of more power.

2.7 Sensitivity analysis

Since the heat source was assumed to be fixed at a specific temperature throughout the whole process optimization, a sensitivity analysis was performed to check the case of utilizing heat sources of different temperatures (45, 65 and 85 °C). The optimized total net power outputs, exergy efficiencies, cold exergy efficiencies, and thermal efficiencies of four different heat source cases are represented in Fig. 2.13. The exergy efficiency increases monotonically according to the temperature of the heat source. Since the exergy inputs of the heat sources are excluded in the calculation of the cold exergy efficiencies, and the amount of power output increases with the temperature of the heat source, the cold exergy efficiencies are enhanced. Likewise, the thermal efficiency shows the same trend as the cold exergy efficiency, but the increase in width is relatively small compared to the cold exergy efficiency. Because all the working fluids selected were only optimized to fit the temperature gliding of the LNG regasification process, a large amount of heat from the heat sources was wasted. Therefore, the thermal efficiencies had small increases as more heat was extracted from the heat source by adopting heat sources with a higher temperature. The exergy efficiencies, which estimate the exergy utilization of both the heat source and heat sink, are placed between the thermal and cold exergy efficiencies. These also increased with the heat source temperature since the power output increase was relatively larger than the amount of the exergy destroyed. This could also be checked by the increasing differences between the cold exergy and thermal efficiencies.

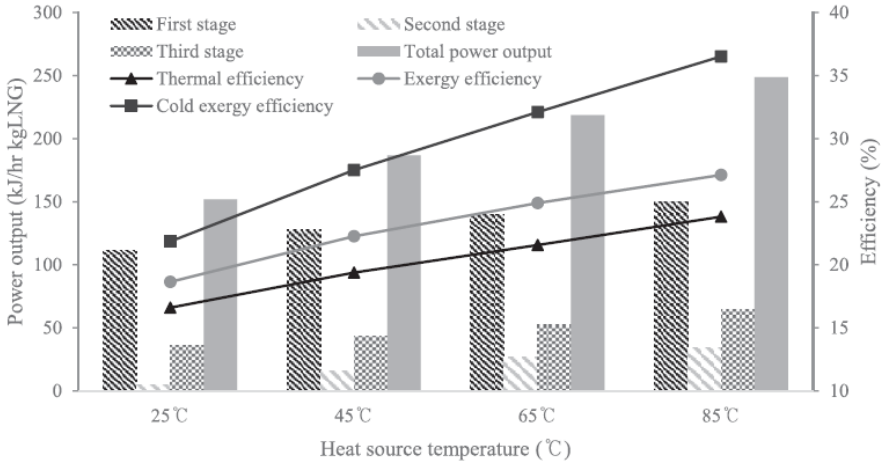

Figure 2.13: Total net power output and efficiencies.

2.8 Conclusions

A novel cascade power generation system utilizing LNG cold exergy was proposed in this study. The proposed cycle adopted binary working fluids for each stage to minimize the exergy destruction in condenser of each stage. To obtain the maximum power output, the best combination set of working fluids was selected through the minimization of the exergy destruction by varying how much cold exergy of the LNG was recovered in the condensers. Then, the working fluid composition, flow rate, and pressure were chosen as variables to minimize the exergy destruction and obtain the maximum power output. After the selection of the working fluids, process optimization was carried out using parameters such as the pressure of the working fluid discharged from the pumps and the intermediate pressure. In addition, using free heat sources in the 25-85 °C range, a sensitivity analysis was carried out to observe the effect on the net power generation according to the heat source temperature.

As a result, the R14-propane combination was found to be the most suitable working fluid for the first stage, and an ethane-n-pentane combination was selected for the second and third stages. The proposed cycle generated 151.78 kJ/h kgLNG under a 25 °C heat source, and showed an exergy efficiency of 18.64%. The performance of the proposed cycle could be increased to 248.79 kJ/h kgLNG, with an exergy efficiency of 27.11% under an 85 °C heat source. According to the result of the exergy analysis, the proposed cycle showed a high performance because of the efficient utilization of the cold exergy. At the place where a large quantity of cold exergy transferred from

the LNG or working fluid to the cycle, the stage showed the highest cold exergy efficiency. Consequently, this reduced the total amount of exergy destroyed and led to a high performance.

Appendix

Table 2.5: Data table streams in proposed process under 25 °C heat source.

	LNG IN	NG OUT1	NG OUT2	S1-1	S1-2	S1-3	S1-4	S1-5	S1-6	S1-7	S1-8
Temperature (°)C	-161	-3.9	-46.5	-134.7	-130.1	-46.5	20	-35.9	20	-33.4	-76.9
Pressure (bar)	1	30	30	0.28	13.7	13.7	13.7	2.285	2.285	0.28	0.28
Vapor Frac	0	1	1	0	0	0.055	1	1	1	1	1
Mass Flow (kg/h)	18.27	8.08	10.19	23.65	23.65	23.65	23.65	23.65	23.65	23.65	23.65
Entropy (kJ/kg K)	-11.15	-6.79	-7.46	-5.48	-5.46	-4.90	-3.85	-3.79	-3.57	-3.49	-3.65
Enthalpy (kJ/kg)	-5073.34	-3832.18	-4768.06	-7518.69	-7514.36	-7409.43	-7133.79	-7173.67	-7117.2	-7167.89	-7203.22

S2-1	S2-2	S2-3	S2-4	S2-5	S3-1	S3-2	S3-3	S3-4	S3-5	LNG1	LNG2	LNG3
-72.7	-72.6	-65.7	20	11.8	-111.5	-111.3	-66.3	20	-20.5	-155.4	-84.9	-84.9
1.71	2.3	2.3	2.3	1.71	0.1	0.9	0.9	0.9	0.1	30	30	30
0	0	0.012	1	1	0	0	0.112	1	1	0	0.622	0
7.2	7.2	7.2	7.2	7.2	6.2	6.2	6.2	6.2	6.2	18.27	18.27	8.08
-8.64	-8.64	-8.54	-6.15	-6.14	-8.84	-8.84	-8.23	-6.21	-6.11	-11.01	-8.51	-9.14
-3072.71	-3072.37	-3052.94	-2482.27	-2494.66	-2839.84	-2839.47	-2724.21	-2196.02	-2257.22	-5052.16	-4643.8	-7203.22

Chapter 3

Robust design of multicomponent working fluid for organic Rankine cycle - consideration on operational uncertainty

3.1 Background

Organic Rankine cycle (ORC) has received intensive attention as a way to generate usable power using waste or renewable heat resources. One common issue on designing ORC is that heat sources or sinks are usually multicomponent mixtures, which diminishes thermal efficiency by increasing the amount of exergy destruction in heat exchangers. Many studies have shown that it is inevitable to use a multicomponent working fluid to achieve high thermal efficiency [1, 2, 3]. This is because, with optimally selected working fluid substances and composition, using a multicomponent working fluid is advantageous in minimizing the exergy destruction in the heat ex-

changer since it better fits the temperature glide of the heat source or sink, compared to single component working fluids. In this context, many studies have been carried out to develop the method for designing the optimal working fluid mixture for ORC. [1, 2, 37, 38, 39, 40, 41, 42] (In this paper, "Design" of working fluid implies selection of substances, determination of composition, and optimization of operating conditions relevant to working fluid such as pressure in each unit of ORC.) Some studies have reported a working fluid optimization method to extract the cold exergy from Liquefied Natural Gas (LNG). They classified the candidate organic materials into several groups (For example, Heavy, Intermediate, and Light) based on normal boiling point. Then several working fluid combinations were made by picking one material from each group prior to composition optimization [1, 2]. In other studies, matching the temperature glide to the heat source or sink, various criteria have been introduced to screen materials for the working fluid mixture, such as environmental impact, net generated power, and thermal stability [37, 38, 39]. Meanwhile, a guideline for selection of working fluid induced from various optimization results has shown that the critical temperature of working fluid mixture should be 30-50 K below the heat source [40]. Mixed integer nonlinear programming (MINLP) has been used as a means to design the optimal working fluid considering extensive combination of substances[41]. Each integer variable of the MINLP was assigned to the usage of each candidate substance so that all the possible combinations could be considered at the same time. Since solving an MINLP problem with its objective function requiring iterative thermodynamic

calculation demands huge computational efforts, Lee et al. suggested that the MINLP should be reduced to a Nonlinear Problem (NLP) by solving it with the Genetic Algorithm (GA), and then the NLP was solved to obtain globally optimal composition using the Branch and Reduce Optimization Navigator (BARON) [41, 43]. Some studies have proposed optimization methods with Computer-Aided Molecular Design (CAMD) to design the optimal working fluid including substances and combinations that have still not been considered with MINLP [42]. As CAMD calculates physicochemical properties using experimentally measured contributions of functional molecular groups, optimization with CAMD can include more substances in the search space [42]. Although the methods described so far have succeeded in significantly improving the efficiency of ORCs, the working fluid obtained as a result of the optimization methods would not be suitable for an actual ORC due to its vulnerability to uncertainties in operating conditions. An ORC using these "optimally designed" working fluid may be in a situation where the net power output decreases severely or its operation becomes infeasible even with a slight change in operating conditions.

Recently, a few studies have been carried out to address such challenges [44, 45, 46, 47]. The effect of the uncertainties existing in the parameters of the Peng-Robinson equation of state on the net power output was analyzed for 20 pure materials when used as ORC working fluids. This work showed that the optimal working fluid could change when uncertainties exist regarding the knowledge of physical properties. [44]. Mavrou et al. suggested a systematic method to design the most robust working fluid from a

prepared working fluid set [45]. Some studies have reported that statistics obtained using Monte Carlo (MC) simulations could be used as the ORC optimization target. Bufi et al. optimized an ORC with 6 pure working fluids assuming that each of the parameters, such as turbine efficiency, heat source temperature, and heat source specific heat, follows a specific distribution [46]. Although it is possible to design the ORC robustly against uncertainties in these ways, it can not be considered as a suitable method for optimizing ORCs using multicomponent working fluids because it uses MC to obtain statistics, which requires excessive computational efforts. Santos-Rodriguez et al. performed scenario-based stochastic optimization to design a multicomponent working fluid. The turbine efficiency and the temperature of the heat source were varied according to the scenarios [47]. In this way, it is possible to design a highly efficient working fluid in various conditions, but a more robust working fluid can be designed if the varying conditions follow distributions rather than discrete scenarios. Moreover, all of the robust design methodologies of the working fluid introduced above does not take into account the possibility of composition changing from the nominal design point, due to thermal degradation[48] or working fluid leakage[49] during ORC operation.

MC simulation can provide the statistical moments required for stochastic optimization, but its slow convergence rate precludes the optimization from obtaining the robust design in a reasonable amount of time. In particular, since the operation of the ORC model involves iterative calculations of thermodynamic equations, even a single realization of ORC simulation requires considerable amount of computational

effort. To address this challenge, in this study, polynomial chaos expansion (PCE) is employed as an efficient way to obtain the statistical moments. PCE is a method of quantifying uncertainty, which allows statistical moments to be obtained accurately with a relatively small amount of simulation compared to MC simulation [50, 51, 52]. Theoretically, PCE has exponential convergence rate, and many studies have reported that PCE requires orders less number of samples than MC simulations [53, 54]. Due to this advantage, PCE has been applied in various fields, such as for analyzing propagation of uncertainty through a system of interest [55, 56, 57, 58], parameter sensitivity analysis [59, 60, 61, 62], and optimization for robust design [63, 64, 65, 66, 67, 68, 69].

The approaches used to obtain PCE can be classified as intrusive and non-intrusive methods. Intrusive methods require manipulation of model equations using the Galerkin method [70] to derive the coefficients of the expansion, which makes implementation of it challenging. On the other hand, non-intrusive methods are easily applicable regardless of the model because it calculates the coefficients from sampled data of the simulation model [71]. For this reason, a non-intrusive method is employed in this study.

To obtain PCE coefficients using non-intrusive methods, multivariate integrals should be computed numerically. Quadrature rules for multi-dimensional integrals may deprive PCE of the benefit of small amount of computation since they involve tensor products of one-dimensional integrals, which increases the number of sample points required for evaluation. The Smolyak sparse grids quadrature can address this

problem by reducing the required samples at the expense of some accuracy [71]. PCE with sparse grid quadrature is less accurate compared to the full grid quadrature, but many studies on application of the PCE have employed sparse grids because it enables efficient construction of the PCE model [72, 73, 74]. The Smolyak sparse grids quadrature is commonly used with the Clenshaw-Curtis rule, which is a one-dimensional quadrature rule, as its nested property is exploited by the multivariate sparse grids rule for efficient numerical integration [71].

In this work, a framework for robustly designing the multicomponent working fluid, which is not susceptible to changes in composition, is presented and implemented to design the optimal working fluid for ORC using LNG cold energy. The proposed method seeks the optimal composition and operating conditions using both the mean and the variance of power output. To exclude the factors that impede safe operation of ORC (such as violation of minimum temperature difference in the heat exchanger and formation of liquid droplet in the expander), the power output is penalized by penalty functions defined in this work. The statistical moments are obtained through the following two steps: First, the required heat exchanger area is calculated by simulation of the ORC model with nominal operating conditions (composition, pump discharge pressure, and expander discharge pressure). Then, simulations are carried out again with the computed area and the operating conditions except the composition fixed at the nominal value. The composition of each substance in the working fluid is assumed to follow a uniform distribution centered at the nominal value. The

PCE model, of which coefficients are calculated by sparse grid quadrature using the Clenshaw-Curtis rule [75] is constructed to obtain the statistics with a small number of simulations [76, 77, 78].

In Section **??**, the formulation of optimization is presented. The issues that should be considered to design robust ORC are described in Section **??**. The objective function and the penalty function to deal with the issues shown in Section **??** are suggested in Section 3.1.1. PCE for obtaining the statistical moments constituting the objective function is described in Section 3.1.2. The optimization procedure introduced in Section **??** is implemented to designing robust ORC using LNG in Section 3.2. At first, the design conditions for the ORC to exploit the cold energy of LNG are described in Section 3.2.1. Prior to implementation, a verification analysis of the statistical moments obtained from PCE with one from MC simulation is performed to ensure the suggested method is reliable in Section 3.2.2. Note that the verification analysis is included in the implementation section because the accuracy of PCE depends on the complexity of a model of interest [52]. In Section 3.2.3, the parameters of the penalty functions defined in Section 3.1.1 are selected based on the repeated optimization result. Among the tested parameters, ones that can guide ORC robust against the uncertainties in the composition are selected. At last, optimization results are presented in Section 3.2.4 showing the robustness of the ORC designed by the proposed method. Also, the optimal working fluid mixture is selected based on the optimization results.

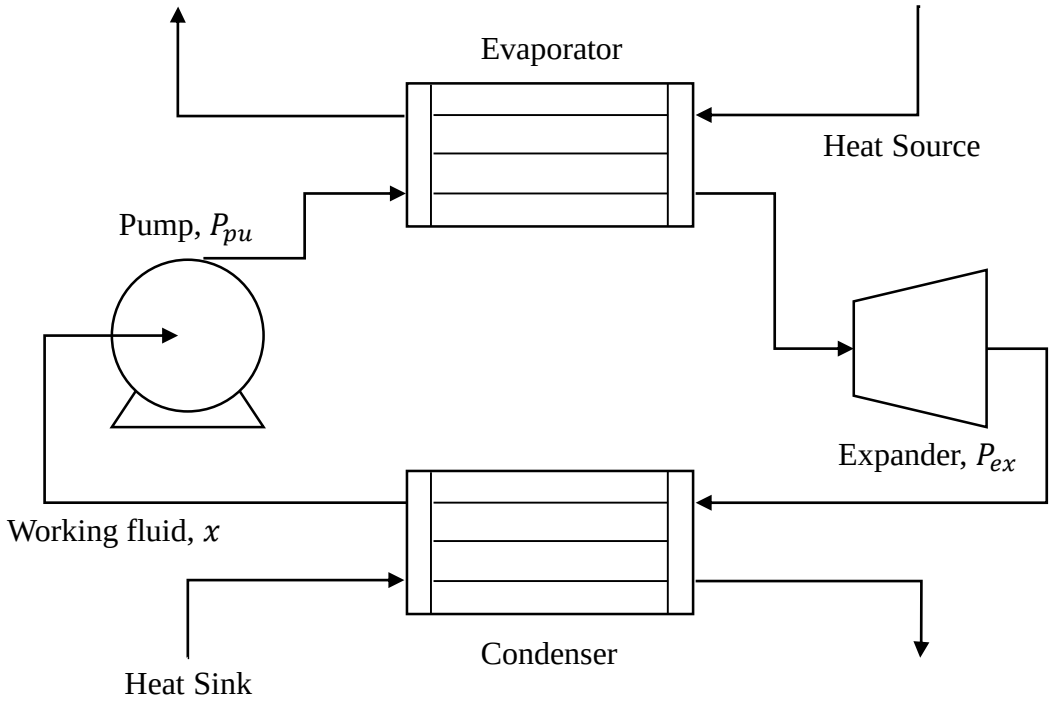

Figure 3.1: Schematic diagram of ORC

To focus on the robust design of the working fluid, the simplest ORC configuration is prepared prior to the optimization procedure. As illustrated in Fig. 3.1, the basic ORC consists of 4 units; condenser, evaporator, pump, and expander. The operating conditions that dominantly affect the ORC design results are known as nominal working fluid composition, x, discharge pressure of pump, P_{pu}, and discharge pressure of expander, P_{ex} [1, 2]. These were used as optimization variables in this study. Other design parameters including expander efficiency and temperature of the heat sink are assumed to be given as specific values. To obtain power output, thermodynamic equations should be computed while satisfying the equality constraints, such as material and energy balance. In addition, there are two conditions that should be avoided when designing ORCs.

- Temperature crossover in the condenser or the evaporator.
- Formation of liquid droplets in the expander.

Because the minimum temperature difference serves as a buffer during the heat exchanger process, preventing the violation of the second law of thermodynamics, a minor violation does not make the immediate operation of ORC infeasible. However, if the minimum temperature difference between the hot and cold streams in the heat exchanger becomes smaller than the design reference, stable ORC operation is threatened, and if it becomes worse, temperature crossover occurs and the efficiency declines seriously. Also, the liquid droplets formed on the surface of the blades cause them to corrode, thereby reducing the efficiency of the expander and ultimately making it in-

feasible to operate the ORC [79]. For these reasons, restricting each of the above two conditions is considered as soft constraints, and the penalty functions which will be defined in Section 3.1.1, are designed to prevent their occurrence.

3.1.1 Evaluation of the objective function

The objective function of the optimal working fluid design problem aims at obtaining the maximum mean and the minimum variance of power output with respect to the penalty functions. The objective function, J, is formulated as a weighted sum of the mean and the negative variance.

$$\text{Maximize} \quad J(x, P_{pu}, P_{ex}) = \mathbb{E}[Y_{pa}] - \kappa\sigma^2[Y_{pa}] \tag{3.1}$$

$$\text{Subject to} \quad \sum_{x_c \in x} x_c = 1 \tag{3.2}$$

where $\mathbb{E}$, σ, and κ are mean, variance, and the weight for variance, respectively. x is the composition vector and x_c is the mass fraction of the component c, where the sum of all the fractions equals 1. The equality constraints other than Eq. (3.2) such as heat and mass balance are omitted to focus on the uncertainty of composition. The power output imposed with penalty, Y_{pa}, is defined by the net power output and the two penalty functions to consider the soft constraints described in Section **??**.

$$Y_{pa} = G_1(\Delta T_{vi}, \gamma_1) G_2(f_l, \gamma_2) Y_{net} \tag{3.3}$$

G_1 is the penalty function for the violation of the minimum temperature difference, and this denotes the amount of the violation, ΔT_{vi} as a variable. γ_1 is the parameter for penalty degree, which determines how important the violation of the minimum temperature difference will be taken into account. G_2 is the penalty function for the formation of the liquid droplets, f_l is the liquid fraction in the outlet stream from the expander, and γ_2 is the parameter for G_2 determining how seriously the liquid droplets

will be considered. Note that both G_1 and G_2 can be defined as any form of functions as long as they restrain the optimal working fluid to satisfy the soft constraints. In this work, G_1 and G_2 are defined as follows:

$$G_1(\Delta T_{vi}, \gamma_1) = \exp(-\gamma_1 \Delta T_{vi}), \quad \gamma_1 > 0 \tag{3.4}$$

$$\Delta T_{vi}(\Delta T_{min}) = (\Delta T_{min}^{ref} - \Delta T_{min}) + |\Delta T_{min}^{ref} - \Delta T_{min}| \tag{3.5}$$

$$G_2(f_l, \gamma_2) = f_g^{\gamma_2} = (1 - f_l)^{\gamma_2}, \quad \gamma_2 > 0 \tag{3.6}$$

where ΔT_{min}^{ref} and ΔT_{min} are the design reference for the minimum temperature difference and the minimum temperature difference resulting from the ORC simulation. f_g is the fraction of gas phase in the outlet stream of the expander satisfying $f_g = 1 - f_l$. The values of the defined penalty functions should monotonically decrease as ΔT_{vi} and f_l increase, thus restraining ΔT_{vi} and f_l from increasing. G_1 is defined as an exponential function taken on a ramp function of ΔT_{min}. Since ΔT_{vi} becomes zero when ΔT_{min} is larger than or equal to ΔT_{min}^{ref}, G_1 becomes one imposing no penalty on the objective function. Also, due to this feature of G_1, it does not offer an incentive to the case of ΔT_{min} larger than ΔT_{min}^{ref}, which may result in low efficiency. When $\Delta T_{min} < \Delta T_{min}^{ref}$, ΔT_{vi} increases and G_1 decreases monotonically as ΔT_{min} decreases. Low G_1 forces the designed ORC to keep ΔT_{min}^{ref} by imposing penalty on the objective function, and the amount of penalty can be adjusted by γ_1.

G_2 is defined to get smaller as f_l approaches one (as f_g approaches zero), and it does not have a value larger than one. Thus, G_2 imposes penalty on the objective function unless f_l is zero. G_2 can be adjusted by the parameter, γ_2, and a high f_l

implies a large penalty because it lowers the G_2 value.

To obtain the statistical moments used in Eq. (3.1), simulations of an ORC model should be computed at x, the nominal composition, and θ, the composition varied from x. Initially at the nominal condition (x, P_{pu} and, P_{ex}), the required heat exchange area, A_h is computed by using Eq. (3.7).

$$A_h = \frac{U\Delta T_{lm}}{Q} \tag{3.7}$$

where U and ΔT_{lm} are the overall heat transfer coefficient and the log mean temperature difference. The heat duty, Q, can be calculated by imposing a design specification on the condenser or the evaporator and using the following equation.

$$Q = m_{hot}(\Delta H_{hot} + C_{p,hot}\Delta T_{hot}) = m_{cold}(\Delta H_{cold} + C_{p,cold}\Delta T_{cold}) \tag{3.8}$$

where the subscripts, hot and $cold$, mean hot and cold streams. m, ΔH, C_p, and ΔT are mass flowrate, required heat for phase change, specific heat, and temperature difference in heat exchanger, respectively. For instance, in case of the condenser, in which heat sink is the cold stream and working fluid is the hot stream, m_{hot}, ΔT_{hot} are specified to make both hot and cold stream condensate and evaporate completely with given m_{cold} and ΔT_{min}^{ref}. All the variables and parameters required for Eq. (3.7) and (3.8) are computed by a commercial process simulator, ASPEN PLUS V10. Once A_h is obtained, sampling abscissas, $\theta^{(i)}$, should be determined to calculate the statistical moments, which simulates changes in composition during ORC operation. θ is assumed to follow an uniform distribution over the range centered at x, and the degree

of change depends on the variation bound I. If an optimization algorithm calls the objective function value at a specific composition, x^*, then

$$\theta \sim \mathbb{U}((1-I)x^*, (1+I)x^*) \tag{3.9}$$

where $\mathbb{U}$ stands for uniform distribution. The determination of θ will be explained in Section 3.1.2. Now that $\theta^{(i)}$ is prepared, Eq. (3.8) is calculated again with the same design specification used at the initial step by varying the mass flow of working fluid. Using the changed mass flow rate due to the changed composition, $Y_{net}(\theta, P_{pu}, P_{ex})$ is obtained from the ORC model. From the ORC model simulated at (θ, P_{pu}, P_{ex}), ΔT_{vi} and f_l can also be obtained, which are required to calculate Y_{pa}. Computation of the mean and variance of Y_{pa} is described in the next section.

3.1.2 Polynomial chaos expansion

PCE is a spectral expansion to quantify uncertainty in outputs propagated from input parameters via orthogonal polynomials. Although MC simulation can also provide statistical moments from sampling, PCE enables them to be obtained with much less amount of samples [80]. In the context of generalized Polynomial Chaos (gPC) [58], if the truncated PCE model of Y_{pa} can be expressed as

$$Y_{pa}(x,\theta) = \sum_{\boldsymbol{\alpha}\in\mathcal{A}} y_{\boldsymbol{\alpha}}(x)\Psi_{\boldsymbol{\alpha}}(\xi(\theta)) + \epsilon \tag{3.10}$$

$$\Psi_{\boldsymbol{\alpha}}(\xi) = \prod_{j=1}^{N_\xi} \psi_{\alpha_j}^{(j)}(\xi_j) \quad s.t. \quad \mathbb{E}\left[\Psi_a \Psi_b\right] = \delta_{ab} \tag{3.11}$$

where x is the composition and N_ξ is the dimension of the vector ξ, which is iso-transformed parameter, θ, with respect to its probability density function f_θ, therefore $\xi_j \sim \mathbb{U}(-1,1)$ when θ is uniformly distributed. Note that the variables P_{pu} and P_{ex} are dropped in Eq. (3.10) for descriptive simplicity. As can be seen in Eq. (3.10), Y_{pa} is approximated based on multivariate orthonormal polynomials, $\Psi_{\boldsymbol{\alpha}}(\xi)$, induced by tensor product of univariate polynomials, $\psi_{\alpha_j}^{(j)}$, which is orthogonal to the probability density function, f_ξ. Some univariate polynomials are known to be orthogonal to corresponding distributions [54], and because θ is assumed to follow a uniform distribution in this study, $\psi_{\alpha_j}^{(j)}$ is selected as the Legendre polynomial. Since $\Psi_{\boldsymbol{\alpha}}(\xi)$ is orthonormal, it satisfies $\mathbb{E}\left[\Psi_a \Psi_b\right] = \delta_{ab}$ (δ_{ab} is the Kronecker delta). $\boldsymbol{\alpha} = \{\alpha_0, \ldots, \alpha_{N_\xi - 1}\}$ are multi-indices and the set $\mathcal{A}$ is the truncated set of the indices. Since the polynomial chaos uses truncated indices for approximation of the original model, truncation error

ϵ is inevitable. The total number of polynomial basis terms for PCE, N_{pc}, is given by $\frac{(N_{\boldsymbol{\xi}}+n_{pc})!}{N_{\boldsymbol{\xi}}!n_{pc}!}$, in which n_{pc} is the order of the polynomial chaos. $y_{\boldsymbol{\alpha}}(x)$ is the deterministic PCE coefficient that needs to be evaluated. Generally, a PCE model with large n_{pc} shows high accuracy in quantifying uncertainties of interest but it increases the number of coefficients to be computed, which requires the evaluation of excessive amount of samples [81]. Thus, n_{pc} should be selected depending on the complexity of the target system [52] and the determination of n_{pc} will be presented in Section 3.2.2.

Nonintrusive spectral projection is chosen among several methods to obtain the coefficient because of its ease of implementation and the characteristic of obtaining accurate results with a small number of samples. Let the operation $< \cdot >$ be the inner product, then $y_{\boldsymbol{\alpha}}(x)$ can be computed by exploiting orthogonality of the polynomial chaos basis.

$$y_{\alpha_k}(x) = \frac{< Y_{pa}(x,\xi), \Psi_{\alpha_k}(\xi) >}{< \Psi^2_{\alpha_k} >} = \int_\Omega Y_{pa}(x,\xi)\Psi_{\alpha_k}(\xi) f_\xi(\xi) d\xi \tag{3.12}$$

where $\Omega \subset \mathbb{R}^{N_\xi}$ is the range of ξ. The right-hand side of Eq. (3.12) can be computed numerically using the quadrature rule.

$$\int_\Omega Y_{pa}(x,\xi)\Psi_{\alpha_k}(\xi) f_\xi(\xi) d\xi \approx \sum_{i=1}^{N} Y_{pa}(x,\xi^{(i)})\Psi_{\alpha_k}(\xi^{(i)}) w^{(i)} \tag{3.13}$$

where N is the total number of samples to compute Eq. (3.13). $\xi^{(i)}$ is the sampling abscissa with corresponding weight $w^{(i)}$. To achieve high accuracy with the minimum number of samples, abscissas and weights are generated by sparse grids utilizing the Clenshaw-Curtis rule [76]. The details about sparse grids can be found in Appendix

3.3.

Once the coefficients of PCE are obtained, the mean and variance can be derived analytically. Due to the orthogonality embedded within the gPC basis, the two statistical moments can be expressed as following equations.

$$\mathbb{E}[Y_{pa}(x)] = y_0(x) \tag{3.14}$$

$$\sigma^2[Y_{pa}(x)] = \sum_{\boldsymbol{\alpha}\in\mathcal{A}\setminus 0} y^2_{\boldsymbol{\alpha}}(x) \tag{3.15}$$

In summary, the statistical moments used in Eq. (3.1) are obtained through the following steps as presented in Fig. 3.2.

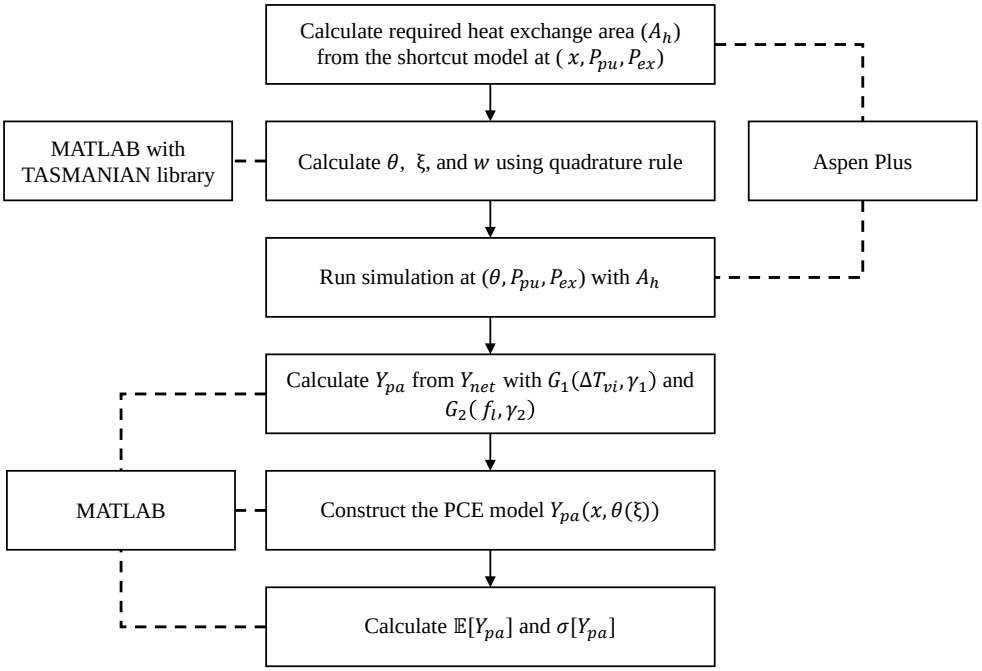

Figure 3.2: Procedure for calculating the statistical moments.

At first, the heat exchange area is calculated at the nominal condition using the ORC model constructed in ASPEN PLUS. Then, θ and ξ are collected using the sparse grid quadrature rule with the Clenshaw-Curtis rule. $\theta^{(i)}$, $\xi^{(i)}$ and $w^{(i)}$ are calculated using toolkit for the adaptive stochastic modeling and non-intrusive approximation (TASMANIAN) [82, 83]. Using prepared A_h and the sampling abscissas, simulation of the ORC model is carried out to obtain Y_{net}, ΔT_{vi}, and f_l. From Eq. (3.3), Y_{pa} is calculated, and then the PCE model for approximating Y_{pa} is constructed. At last, $\mathbb{E}[Y_{pa}]$ and $\sigma[Y_{pa}]$ can be obtained analytically from Eq. (3.14) and (3.15).

3.2 Implementation

3.2.1 ORC with LNG heat sink using ternary working fluid

The proposed optimization strategy was implemented on the working fluid design for an ORC using LNG as heat sink. LNG should be evaporated before it is delivered to the places of use and in general, the cold energy from the evaporation process is wasted. ORC can convert the cold energy into electronic energy by using the LNG to condensate the working fluid of ORC. Since LNG is a mixture heat sink, it has been repeatedly reported from previous studies that a multicomponent working fluid should be adopted to obtain the optimal power output [1, 2, 3]. In this study, four ternary working fluid combinations, which are considered as optimum but not robust, are chosen as candidate mixtures based on the work of Lee et al. [1]. They conducted an investigation on 12 working fluid combinations and concluded that the mixture fluids containing R23 and R14 show minimum irreversibility in the condenser. Irreversibility can be calculated using enthalpy, h, and entropy, s.

$$\Delta e = e_{in} - e_{out} = (h_{in} - h_{out}) - T_0(s_{in} - s_{out}) \tag{3.16}$$

$$Irr = m_{wf}\Delta e_{wf} + m_{LNG}\Delta e_{LNG} \tag{3.17}$$

where the subscripts in and out denote the streams flowing into and out of the condenser, respectively. Subscripts wf and LNG represent the working fluid stream and the LNG stream. e and Δe are the exergy of a stream per unit mass and its amount of change caused by ORC condenser. T_0 is the reference temperature which is set

to 298.15K. Irreversibility, Irr, which implies the exergy destruction occurring in the condenser can be measured by Eq. (3.17), which consists of products of mass flowrate, m, and the exergy change, Δe. To compare the amount of exergy destruction with respect to unit mass of LNG, irreversibility in Table 3.1 is given by $\frac{Irr}{m_L NG}$. Table 3.1 represents the results of irreversibility minimization using the working fluid combination candidates [1].

Table 3.1: Candidate combinations for working fluid mixture

Combination	Substance	Composition	Pressure (bar)	Irreversibility (kJ/kg LNG)
$wk1$	R30, R23, R14	0.068 : 0.680 : 0.252	1.6	90.41
$wk2$	R601, R23, R14	0.227 : 0.707 : 0.067	1.44	89.16
$wk3$	R245fa, R23, R14	0.092 : 0.624 : 0.284	1.70	95.49
$wk4$	R236fa, R23, R14	0.303 : 0.545 : 0.152	1.55	107.24

The pressure, temperature and mass flow rate of LNG are set to be 30 bar, -167 °C, and 1620 tonne/hr, respectively. The composition of LNG is listed in Table 3.2. The heat source is assumed to be low-pressure steam drawn from a pulverized coal power plant, of which pressure and temperature are 0.247 bar and 67.3 °C respectively. Also, it is assumed that the amount of heat source is sufficient enough to vaporize all of the working fluid, and the temperature of the vaporized working fluid is assumed to be 66.3 °C. More details about the ORC operating conditions can be found in the previous study [1].

Table 3.2: Composition of LNG

Component	Mole fraction
N_2	0.0007
Methane	0.8877
Ethane	0.0754
Propane	0.0259
n-butane	0.0056
i-butane	0.0045
n-pentane	0.0001
i-pentane	0.0001

As the working fluid candidates are ternary mixtures, the composition, x, is composed of three mass fractions. But its dimension is two because the composition has to satisfy the constraint Eq. (3.2) even when it varies due to uncertainty. Thus, one of the mass fractions is set to be determined according to the other varied fractions, and the upper bound for the sum of the other fractions is set not to exceed 1, namely,

$$\theta_3 = 1 - (\theta_1 + \theta_2) \tag{3.18}$$

$$1 \geq (1 + I)(x_1 + x_2) \geq \theta_1 + \theta_2 \tag{3.19}$$

For convenience of representation, the indices $1, 2$, and 3 for x_c represent heavy, intermediate, and light component in the working fluid, respectively. The isentropic efficiency for both pump and expander is set to 0.72. To analyze the impact of the composition variation when varied 5% and 10% from its nominal point are assumed, I is set to 0.1 and 0.05. The optimization with $I = 0$ is also performed to test the working fluids designed without consideration of uncertainty. The weight value for variance, κ, used in the objective function is set to 0.5. The simulation for computing the power output is carried out using ASPEN PLUS V10 and the Peng-Robinson model is employed as the property model, which shows high accuracy in predicting behaviors of hydrocarbon compounds [84]. The optimization is performed by Matlab 2018a using the Bayesian optimization algorithm[85] in order to efficiently solve the time-consuming and nonlinear problem. One evaluation of the objective function takes 30 to 300 seconds depending on the operating condition under the computational environment of 64-bit Intel® Core™ i7-8700K CPU 3.70GHz processor.

3.2.2 Precision test for PCE

Prior to performing optimization, the statistical moments obtained with PCE were tested to determine the order of PCE and the number of samples required to construct the PCE model. The higher the order of PCE, the higher the accuracy [76], but since the required number of samples increase simultaneously, PCE with high order is not suitable for optimization that requires many iterations. In order to perform optimization efficiently in a reasonable amount of time, accurate statistics should be obtained by PCE with low order. The accuracy test results for various orders of PCE according to the number of required samples are represented in Fig. 3.3. The mean and the variance of Y_{pa} obtained by PCE were compared to those by 10^4 MC simulations. The working fluid combination used for the test is $wk1$ and the operating conditions, x, P_{ex}, and P_{pu} are selected at $x = (x_1, x_2, x_3) = (0.056, 0.602, 0.342)$, $P_{ex} = 2.56$ bar, $P_{pu} = 29.4$ bar.

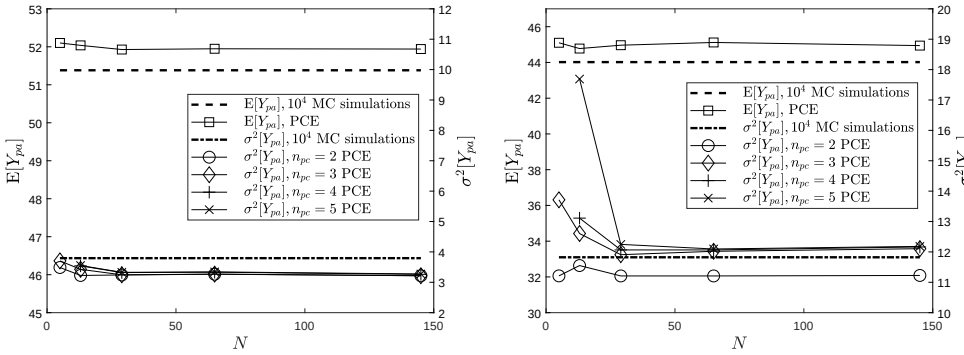

(a) $I = 0.05$ (b) $I = 0.1$

Figure 3.3: Precision test for PCE with MC simulation

Note that the variance obtained by PCE of which order is higher than or equal to 4 using 13 samples were omitted from Fig. 3.3 due to their large deviation from the MC simulation result. The number of samples, N, is determined by the level of sparse grids which is described in Appendix 3.3. The mean value depends only on the number of samples and not on the order of PCE since it is calculated by the first coefficient of PCE which is shared with all the PCE order (see Eq. (3.14)). $\mathbb{E}[Y_{pa}]$ shows only a slight difference with regards to the number of samples. When I equals 0.05, no significant difference in accuracy is observed in both mean and variance, but the error for $\sigma[Y_{pa}]$ becomes large when the number of samples is below a certain value for $I = 0.1$. Also, PCE with $n_{pc} = 2$ shows less accurate results in the calculation of variance than PCE with $n_{pc} = 3$ but no significant difference is observed when n_{pc} is higher than 3. In the remaining part of the paper, according to the test result, n_{pc} and the required N will be fixed at 3 and 65, which gives the most accurate prediction of variance with small number of required samples. Mean squared error of the selected n_{pc} and the required N is 1.94 for $\mathbb{E}[Y_{pa}]$ and 0.15 for $\sigma^2[Y_{pa}]$.

3.2.3 Influence of penalty function

The penalty applied to the objective function determines how robust the designed working fluid will be. The larger the parameters in Eq. (3.4) and (3.6) are, the more robust the working fluid is, but too large a penalty can lead to excessive degradation of efficiency. For this reason, the analysis of the optimization results was performed to find the appropriate γ_1 and γ_2. $wk1$ was used to analyze the penalty parameters. In order to grasp the trend of the influence of the parameter on the objective function value, each parameter was altered from 1 to 9, and their results were analyzed.

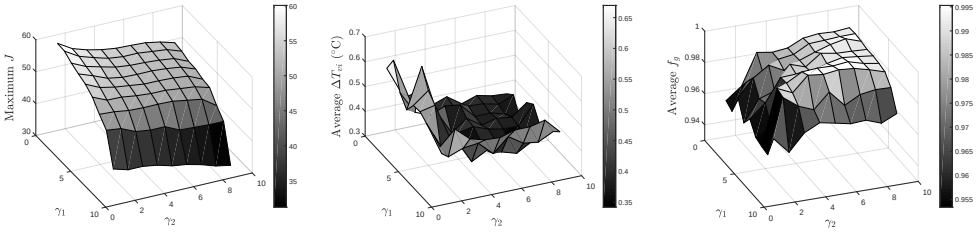

(a) Maximum J (b) Average ΔT_{vi} (c) Average f_g

Figure 3.4: Optimization result according to penalty parameters.

As represented in Fig. 3.4, the value of the objective function, J, decreases as γ_1 and γ_2 become large but the violation trend of the soft constraints changes irregularly. One characteristic which can be observed in Fig. 3.4 is that both average ΔT_{vi} and f_g depend on both γ_1 and γ_2. It seems that the large penalty parameter for the violation of minimum temperature difference, γ_1, can not mitigate ΔT_{vi} if γ_2 is too small or too large. This is because ΔT_{vi} and f_g are inter-dependent when running ORC simulations. However, the range of γ_1 and γ_2 resulting in both low ΔT_{vi} and high f_g can be found in Fig. 3.4 (darker area in Fig. 3.4b and brighter area in Fig. 3.4c). The penalty parameters were set to $\gamma_1 = 5$ and $\gamma_2 = 7$, which gives the highest J value within the tested range.

3.2.4 Results and discussion

Robustness analysis

Using a working fluid combination $wk1$, MC simulations were performed to compare and observe how sensitive the working fluids designed under $I = 0.1$, 0.05 and 0 are to the uncertainty in the composition. The composition and pressure of the working fluid used in the analysis are the result of optimization by the proposed method and can be found in Table 3.6. The simulation results were analyzed for the cases that the composition uniformly deviates from the nominal points within 5%, 10%, and 20% variation bounds ($I_a = 0.05$, $I_a = 0.1$, and $I_a = 0.2$). Note that both I_a and I are values representing the level of uncertainty existing in the composition, but I_a must be distinguished from I in that it is used in the MC simulation for the robustness analysis and I is used in the design phase of the working fluid. In particular, analysis with $I_a = 0.2$ was carried out to show a situation where the composition is larger than predicted at the design stage. Table 3.3 - 3.5 represent the simulation results.

Table 3.3: Robustness test for $wk1$ by MC simulation with $I_a = 0.05$

I	Y_{net}	ΔT_{vi}	f_g	Irreversibility
0	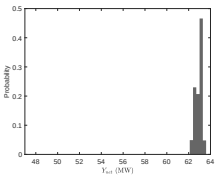	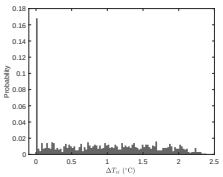	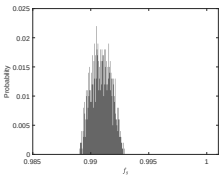	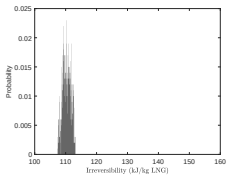
0.05	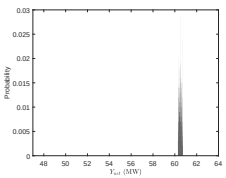	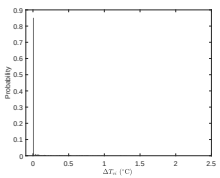	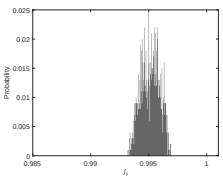	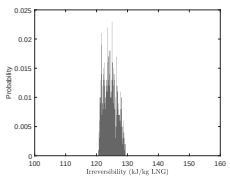
0.1	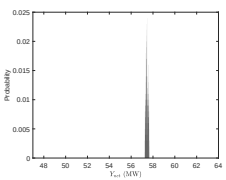	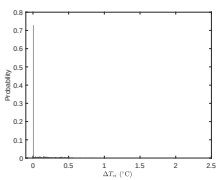	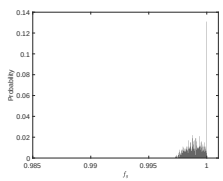	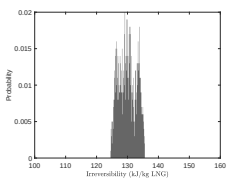

Table 3.4: Robustness test for $wk1$ by MC simulation with $I_a = 0.1$

I	Y_{net}	ΔT_{vi}	f_g	Irreversibility
0	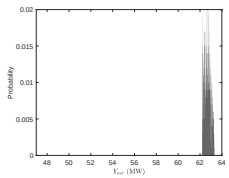	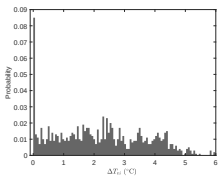	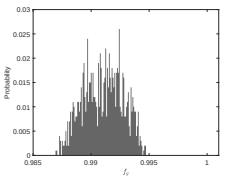	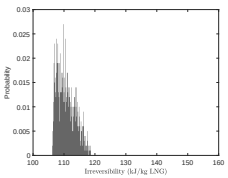
0.05	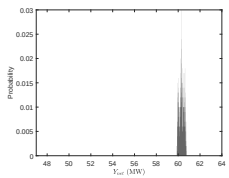	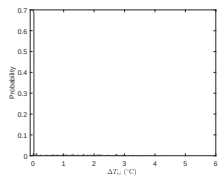	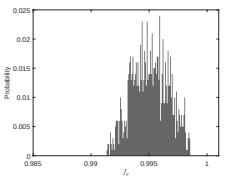	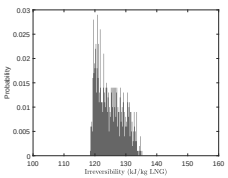
0.1	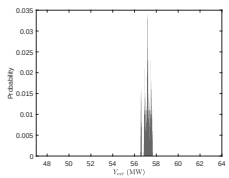	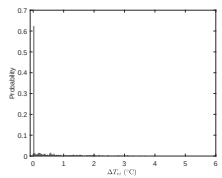	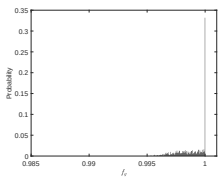	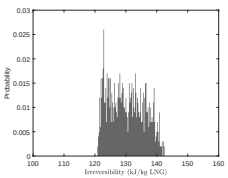

Table 3.5: Robustness test for $wk1$ by MC simulation with $I_a = 0.2$

I	Y_{net}	ΔT_{vi}	f_g	Irreversibility
0	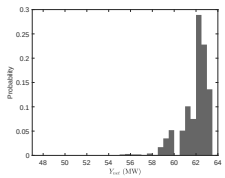	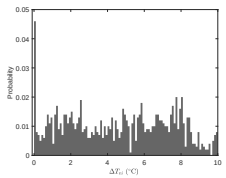	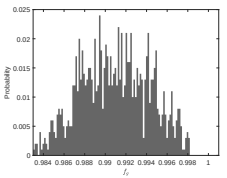	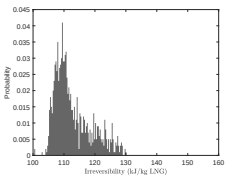
0.05	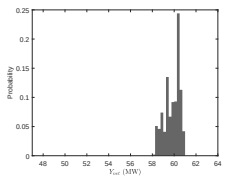	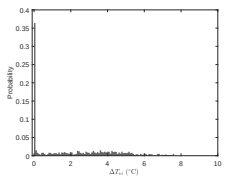	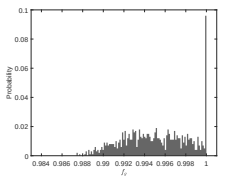	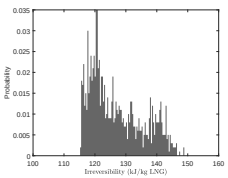
0.1	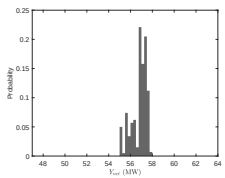	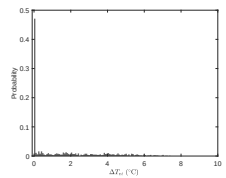	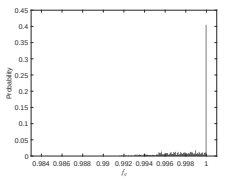	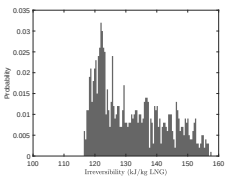

It can be seen that the larger the uncertainty that was considered in design, the smaller the Y_{net} produced by ORC is. The reason is that assuming large uncertainties results in the design of working fluids becoming conservative from operational risks. This can be checked from the results of irreversibility. The values of irreversibility get larger as higher uncertainties in composition are assumed. This implies large I forces ORC to have large gap between the temperature glides of the working fluid condensation process and LNG evaporation process, which leads to large destruction of LNG cold exergy. However, the violation of the reference minimum temperature difference, ΔT_{vi}, can be minimized in the cost of irreversibility as can be seen in the columns for ΔT_{vi} in Table 3.3 - 3.5. For ΔT_{vi}, if the uncertainty of composition is considered, the size of I value is important, and even small I can mitigate the risk of temperature crossover.

The design case of $I = 0.1$ is the most secure from the liquid droplet formation compared to the other design cases because its f_g value is always closest to 1 regardless of the degree of the variation bound. When the variation bound is larger than the value predicted at the design stage ($I_a = 0.2$), f_g of the working fluid designed under $I = 0$ is the most widely distributed. This shows that design without consideration on robustness is vulnerable to changes in operating conditions.

As shown in Table 3.5, the results assuming larger I_a at the design stage show the same trends appearing in Table 3.3 and Table 3.4 except for the fact that all the distributions become relatively wider. The proposed method achieves the robustness

in the working fluid by "conservative" design meaning that it purposely lowers the ORC performance by recovering less LNG exergy, thereby secures a buffer that does not violate the soft constraints even if the composition changes. Therefore, stable ORC operation is possible if the deviation of composition results in a change in output that the buffer can afford. For this reason, the design case of $I = 0.1$ can show $\Delta T_{vi} \sim 0$ and $f_g \sim 1$ in the most of the simulations when $I_a = 0.2$.

Selection of robust working fluid

Now that the proposed design strategy is proven to be effective, optimization using the approach was performed with and without uncertainty in the composition for the four candidate working fluid combinations listed in Table 3.1. The optimization results are summarized in Fig. 3.5 and the details are listed in Table 3.6.

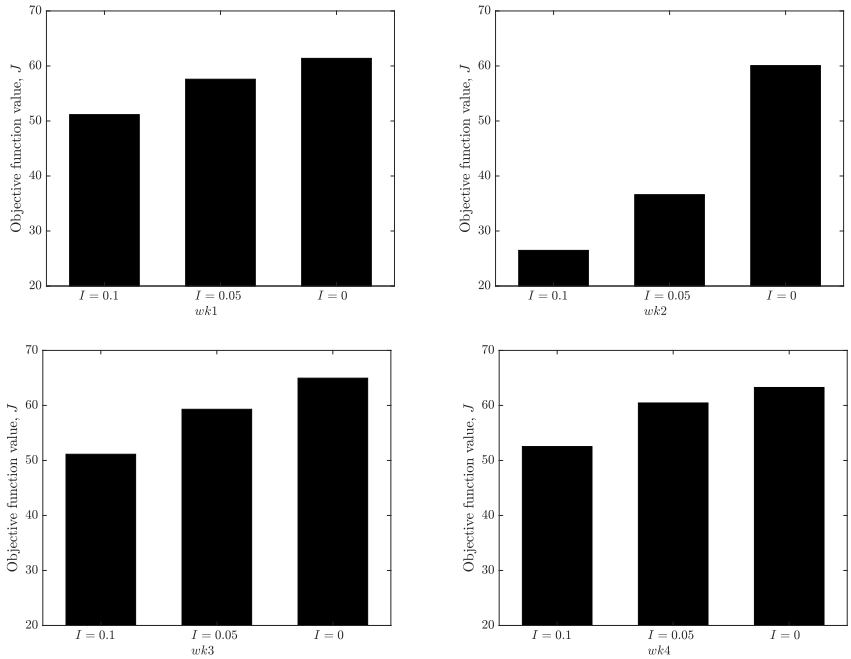

Figure 3.5: Optimization results for working fluid combinations with I =0, 0.05, and 0.1.

Table 3.6: Working fluid design result

Combination	Constituent materials	I	J	Y_{net} (MW)	$\mathbb{E}[Y_{pa}]$	$\sigma^2[Y_{pa}]$	$x = (x_1, x_2, x_3)$	P_{pu} (bar)	P_{ex} (bar)
		0	-	61.38	-	-	(0.0441, 0.5607, 0.3952)	28.90	2.93
$wk1$	R30, R23, R14	0.05	57.59	60.81	58.17	1.15	(0.0402, 0.5696, 0.3901)	28.99	3.47
		0.1	51.11	57.73	53.39	4.57	(0.0413, 0.6132, 0.3455)	25.32	3.29
		0	-	60.06	-	-	(0.1047, 0.7493, 0.1460)	14.33	1.01
$wk2$	R601, R23, R14	0.05	36.60	48.01	41.56	9.92	(0.2288, 0.6421, 0.1292)	11.09	1.35
		0.1	26.48	35.17	28.98	5.05	(0.3364, 0.5654, 0.0982)	7.38	1.57
		0	-	64.96	-	-	(0.0586, 0.5668, 0.3746)	34.60	2.73
$wk3$	R245fa, R23, R14	0.05	59.30	63.36	60.31	2.04	(0.0528, 0.6937, 0.2535)	28.11	1.82
		0.1	51.12	60.42	53.87	5.50	(0.0422, 0.6611, 0.2966)	25.78	2.34
		0	-	63.26	-	-	(0.2166, 0.7498, 0.0337)	24.84	0.78
$wk4$	R236fa, R23, R14	0.05	60.44	61.91	60.68	0.48	(0.1350, 0.7171, 0.1480)	28.00	1.13
		0.1	52.28	54.95	52.52	0.46	(0.6892, 0.2878, 0.0230)	8.23	0.25

Y_{net} in Table 3.6 represents the net power output calculated at the nominal point without consideration on the penalties. The results for $I = 0$ in Fig. 3.5 were calculated not from statistical moments but only from the nominal value since there was no uncertainty to consider. Among the design cases using different levels of uncertainties, the high objective function value, J, for $I = 0.1$, should be used as the optimal criterion for selection of robust working fluid as it implies that the ORC can produce high power output under the worst uncertainty assumption.

The optimal working fluid that shows the highest J was turned out to be $wk4$, thus it is selected as the optimal working fluid in this study. Although ORC using $wk3$ can produce more net power output, Y_{net} than one using $wk4$, the working fluid $wk4$ is more robust against the uncertainty in composition.

Meanwhile, as $\mathbb{E}[Y_{pa}]$ represents the mean of the power outputs imposed with penalties at varied composition, the difference between Y_{net} and $\mathbb{E}[Y_{pa}]$ can be considered as a measure of the amount of penalty imposed. That is, the small difference between Y_{net} and $\mathbb{E}[Y_{pa}]$ indicates that an ORC using the working fluid barely violates the soft constraints even when the composition changes from its nominal value, and therefore the working fluid is robust. The selected working fluid, $wk4$, shows the least difference between Y_{net} and $\mathbb{E}[Y_{pa}]$. This concludes that the selected working fluid is the most robust against the operational risks considered in this study. The variance of power output, $\sigma^2[Y_{pa}]$, serves to ensure that the selected working fluid has such robust properties through the objective function value. This is because $\sigma^2[Y_{pa}]$ value

allows J to reflect the amount of the ORC output deviating from $\mathbb{E}[Y_{pa}]$ by the penalty functions. If the objective function does not consider $\sigma^2[Y_{pa}]$, which is the weight for variance, κ, is zero, then $wk3$ can be selected as the optimal working fluid. This is undesirable in that violation of the soft constraints can be relatively high, so the stable operation of ORC can be threatened.

For all the cases, as variation of the composition increases, the maximum value of the objective function J decreases, but there is a difference in how much it affects J. $wk2$ is found to be most affected by the uncertainty. Also, $wk2$ designed under $I = 0.1$ shows the lowest J value among the working fluid candidates. Therefore, it can be concluded that $wk2$ should be excluded from consideration of the working fluid for robust ORC operation.

To compare the influence of the uncertainty in composition on the worst working fluid, $wk2$ and the optimally selected working fluid, $wk4$, MC simulations were performed using the design case under no uncertainty, $I = 0$. The deviation of composition for MC simulation, I_a, is set to 0.1. Fig. 3.6 and Fig. 3.7 represent the results for $wk2$ and $wk4$, respectively.

f_g values for $wk2$ is more concentrated in 1 than the values for $wk4$, which implies the most of ORC simulations using $wk2$ does not result in the formation of liquid phase in the expander. Liquid phase in the expander can be observed for ORC simulations using $wk4$, but the amount of penalty is not significant due to f_g is distributed close to 1 (f_g is distributed over [0.994, 0.998]). On the other hand, the amount of

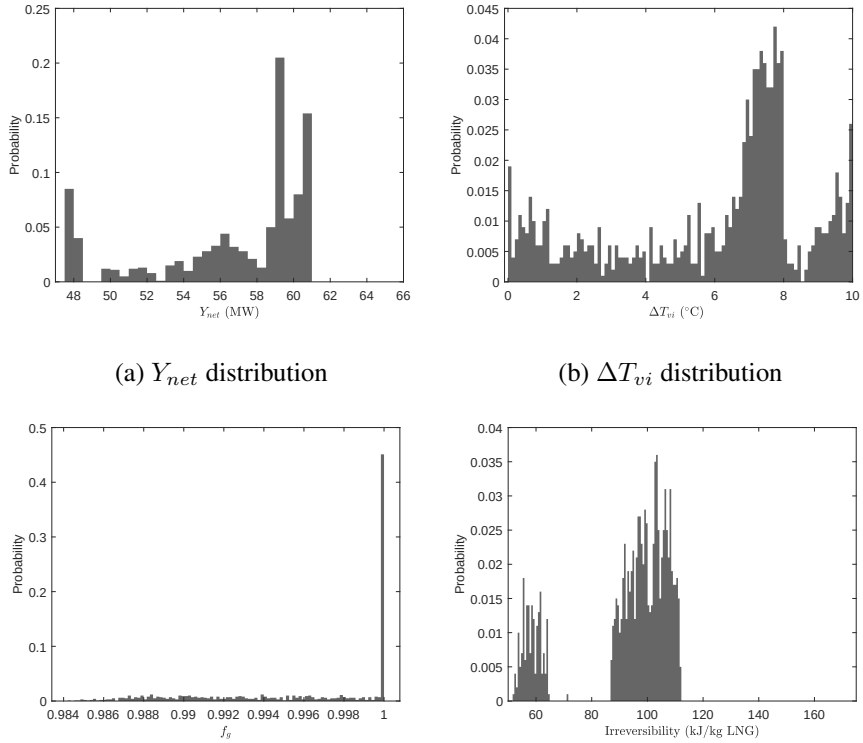

(a) Y_{net} distribution

(b) ΔT_{vi} distribution

(c) f_g distribution

(d) Irreversibility distribution

Figure 3.6: Robustness test for $wk2$ designed under $I = 0$

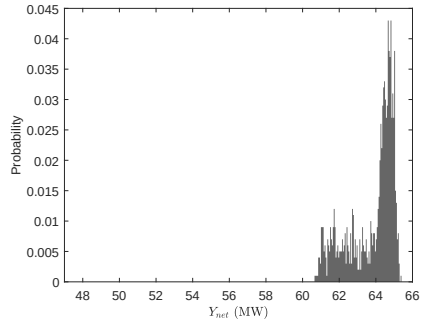

(a) Y_{net} distribution

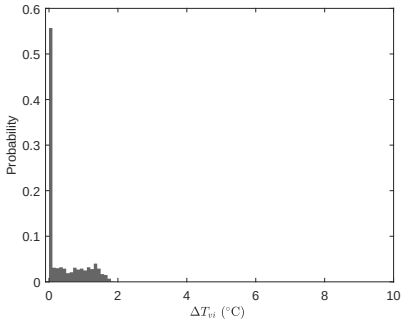

(b) ΔT_{vi} distribution

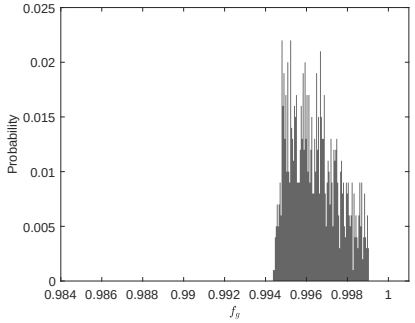

(c) f_g distribution

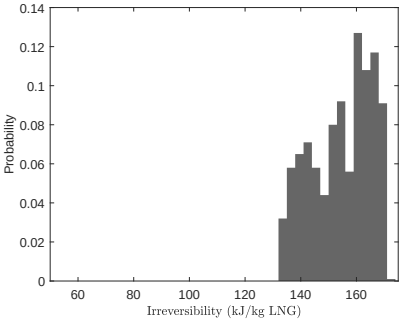

(d) Irreversibility distribution

Figure 3.7: Robustness test for $wk4$ designed under $I = 0$

the reference minimum temperature violation, ΔT_{vi}, for $wk2$ is large and distributed broadly compared to $wk4$. Since the minimum temperature in the condenser using $wk2$ is smaller than ΔT_{min}^{ref}, the irreversibility can be mitigated but the large penalty is imposed on the objective function value. This property of $wk2$ makes it sensitive to composition uncertainty. Also, a discontinuity is observed in irreversibility distribution for $wk2$. This is because when the composition varies from its nominal condition, the mass flowrate of the working fluid is adjusted largely to satisfy Eq. (3.8). This results in broad distribution of irreversibility and Y_{net}.

ORC using $wk4$ shows large irreversibility compared to one using $wk2$ but barely violates the reference minimum temperature difference. This indicates the temperature glide of condensation process of $wk4$ is relatively insensitive to composition change. Also, the distribution of Y_{net} and irreversibility are narrower than the distributions for $wk2$. These characteristics contributed to robustness of $wk4$.

3.3 Conclusion

A method to design a robust working fluid mixture has been proposed. The proposed method seeks the optimal composition and operating condition yielding the maximum mean power output with the lowest operational risk. The penalty functions are devised to design a working fluid capable of stable operation of ORC under uncertainty in composition. PCE with the sampling points, obtained by the sparse grids, enables the statistical moments to be calculated efficiently. The statistical moments obtained from the PCE showed high accordance with the MC simulation result enough to be used for the optimization.

It has been shown that the working fluid designed assuming uncertainty in the composition is insensitive to the varying composition. The robustness of the designed working fluids can be achieved as they formed a buffer that mitigates the risks of violating the soft constraints in the cost of the increased exergy destruction. The selected optimal working fluid combination was $wk4$, which is composed of R236fa, R23, and R14. $wk4$ shows the highest objective function value when there is 10% variation in the composition. It is a notable result because $wk4$ showed the highest irreversibility in the previous study as can be seen in Table 3.1. This indicates that selection of the optimal working fluid should consider the uncertainties, otherwise the designed ORC would be vulnerable to the operational risks. The proposed method can be easily implemented to designing any ORC working fluids as it uses the nonintrusive spectral method to construct the PCE model.

The future work required to further refine the method proposed in this work can be classified as two works: First, the target configuration of ORC model should be updated referring to recent developments of ORCs. The ORC model used in this study has the simplest configuration to reduce the burden of computation. The units commonly used to improve the efficiency of ORCs such as recuperation units and superheaters, should also be included in the ORC configuration in order for the proposed method to be generally used in designing ORC working fluids. Second, more uncertainties that can affect the operation of ORC should be considered. Besides the composition, other variables and parameters such as the design pressure and the efficiency of the expander may not be constant during the operation of ORC. A study considering these uncertainties would allow the proposed method to obtain further robust working fluids.

Appendix

Let $\mathcal{U}^l$ denote the interpolants of the function $F : [-1,1]^d \rightarrow \mathbb{R}$, where $F(\xi) = Y_{pa}(x,\xi)\Psi_{\alpha_k}(\xi)$. x is omitted in $F(\xi)$ since the coefficients are evaluated at a fixed x. For one-dimensional case, $\mathcal{U}^{m(l)}$ can be expressed as:

$$\mathcal{U}^l(F) = \sum_{j=1}^{m(l)} F(\xi_j) \cdot a_j^l \tag{3.3.1}$$

in which $l \in \mathbb{N}$, $a_j^l \in C([-1,1])$, and $\xi_j \in [-1,1]$. The numerical quadrature is

$$\int F(\xi) f_\xi(\xi) d\xi = \sum_{j=1}^{m(l)} w_j^l F(\xi_j) \tag{3.3.2}$$

$$w_j^l = \int a_j^l f_\xi(\xi) d\xi \tag{3.3.3}$$

In case that the Clenshaw-Curtis quadrature is used, ξ_j is given by the Chebyshev nodes, that is, $\xi_j = \cos\left(\frac{(j-1)\pi}{m(l)}\right), j = 1,\ldots,m(l)$. a_j^l is the Lagrange basis function, which is given by $a_j^l = \prod_{k=1,k\neq j}^{m(l)} \left(\frac{\xi-\xi_k}{\xi_j-\xi_k}\right)$. In general, the Clenshaw-Curtis rule adopts $m(0) = 1$ and $m(l) = 2^l + 1$ for $l > 1$ to have nested property in the quadrature nodes [83, 86]. The multivariate interpolation is given by the tensor product formulae.

$$\left(\mathcal{U}^{l_1} \otimes \cdots \otimes \mathcal{U}^{l_d}\right) = \sum_{j_1=1}^{m(l_1)} \cdots \sum_{j_d=1}^{m(l_d)} F(\xi_{j_1}^{l_1}, \ldots, \xi_{j_d}^{l_d}) \cdot (a_{j_1}^{l_1} \otimes \cdots \otimes a_{j_d}^{l_d}) \tag{3.3.4}$$

where $l_1,\ldots,l_d \in \mathbb{N}$ and $j_1,\ldots,j_d \in \mathbb{N}$. The quadrature using Eq. (3.3.4) which is associated with the full grids requires to evaluate $m(l_1)\ldots m(l_d)$ function samples.

Meanwhile, the Smolyak formula, $\mathcal{B}(q,d)$, reduces required samples by linear combinations of product formulae. The level of sparse grids, q, is an integer, which

determines the number of samples to be evaluated. For $q \geq d$,

$$\mathcal{B}(q,d) = \sum_{|\mathbf{l}|\leq q} (\Delta^{l_1} \otimes \cdots \otimes \Delta^{l_d}) \tag{3.3.5}$$

$$\Delta^l = \mathcal{U}^l - \mathcal{U}^{l-1}, \quad \mathcal{U}^0 = 0 \tag{3.3.6}$$

where $|\mathbf{l}| = l_1 + \cdots + l_d$ and $\mathbf{l} = (l_1, \ldots, l_d) \in \mathbb{N}^d$. $\mathcal{B}$ can be expressed as following, which is equivalent to Eq. (3.3.5).

$$\mathcal{B}(q,d) = \sum_{q-d+1\leq|\mathbf{l}|\leq q} (-1)^{q-|\mathbf{l}|} \cdot \binom{d-1}{q-|\mathbf{l}|} \cdot \left(\mathcal{U}^{l_1} \otimes \cdots \otimes \mathcal{U}^{l_d}\right) \tag{3.3.7}$$

When the set of nodes required for $\mathcal{U}^l$ is Ξ^l, (i.e. $\Xi^l = \{\xi_1^l, \ldots, \xi_{m(l)}^l\}$), the sparse grid used by Eq. (3.3.7) is given by

$$\mathbf{\Xi}(q,d) = \bigcup_{|\mathbf{l}|\leq q} (\Xi^{l_1} \times \cdots \times \Xi^{l_d}) \tag{3.3.8}$$

Therefore, the number of samples required by the q level of sparse grids for d dimensional formula, $N(q,d)$, is

$$N(q,d) = \sum_{|\mathbf{l}|\leq q} (m(l_1) \cdots m(l_d)) \tag{3.3.9}$$

For more details including the approximation error and quadrature examples, readers may read the literatures on the sparse grids [86, 87, 83, 88].

Chapter 4

Robust design of multicomponent working fluid for organic Rankine cycle - consideration on more uncertainties

4.1 Background

This chapter introduces a method to extend the dimension of the uncertain variables considered in the robust optimization procedure to higher dimensions. The only uncertainty taken into account in Chapter 3 was the composition varying during operation of ORC, which affects stable operation. However, the uncertainties reported to have an impact on the flexibility of ORC operation include more operating conditions such as the isentropic efficiency of expanders and the temperature of heat sources [47]. Especially, the temperature of heat source has a serious impact on ORC operation because the heat energy to vaporize the working fluid may be diminished, which can result

in significant reduction of power output and formation of liquid droplet in expanders [45]. Therefore, in order to design a robust ORC, varying temperature of heat source should be considered in addition to composition, and further, uncertainties of the thermodynamic property model used in ORC model should be considered. Frutiger et al. pointed out that the parameters such as critical temperature and critical pressure of each substance in working fluid mixture have an influence on ORC operation which can not be ignored [44].

Designing ORC considering all the uncertainties listed above may be an infeasible optimization problem due to the curse of dimensionality. In case that the statistical moments in Eq. (3.1) are calculated by MC simulations, the number of sample points to be collected is so large that a single evaluation of the statistical moments needs days of computation. A PCE analysis described in Chapter 3 for high dimensional uncertain variables and parameters requires the exponentially increasing number of function values to compute the PCE coefficients according to the dimension. Although the sparse grid quadrature mitigates the burden of computation by reducing the required samples points for numerical integration, still, it should collect huge amount of data. For instance, if d, the dimension of considered uncertain variable vector, is nine and q, the level of sparse grids is seven, 26,017 samples points are required to construct a PCE model for a single evaluation of the statistical moments. Since the robust optimization needs repeated evaluation of the objective function, which leads to excessive amount of the total realization of the ORC model, the same method used in Chapter 3 should

be replaced with a more efficient way to measure the statistical moments.

A surrogate model is an attractive option to analyze heavy models due to its explicit representation of the dependence of an output on input variables. Once a surrogate model is obtained, the computational efforts for the rest of the optimization procedure dramatically decreases. Numerous studies on optimization using surrogate models have been reported to prove the usefulness of it if the constructed surrogate model shows low validation error [89, 90]. Among the methods to construct a surrogate model, PCE is the most commonly used method when the use of the surrogate model is associated with uncertainty quantification of the original model. Note that the PCE model used in Chapter 3 can be classified as a surrogate model predicting the objective function depending on the uncertainty in the working fluid composition. However, the PCE models constructed in Chapter 3 did not predict the relation between the objective function and the optimization variable so it needed to be constructed at every point called by the optimization algorithm. This way succeeded in finding the robust design in Chapter 3 where only low dimensional uncertainties are considered. Now that the uncertainty extends a higher dimension (nine-dimension in this Chapter), the same method is no longer efficient and a new surrogate model embedded with the dependence of the objective function on both optimization points and uncertain parameters is required. This can be achieved by combining a PCE model to quantify uncertainties with a proper regression model to predict the value for the objective function at a nominal design point.

Some studies have tried to combine a PCE model with other regression models [91, 92, 68]. Schobi et al. represented the way to construct the kriging model based on PCE [91]. They let the kriging model, which predicts the behavior of the original model as a realization of a Gaussian random process, approximate the local behaviors on the model, while the global dependence is predicted by the PCE model. Mai et al. developed a nonlinear autoregressive exogenous model (NARX) based on PCE to approximate time-dependent nonlinear models [92]. They employed least angle regression (LARS) to obtain the PCE coefficients efficiently and reported that the constructed surrogate model shows high accuracy in predicting propagation of input uncertainties. Shen et al. suggested a method for stochastic optimization using the surrogate model constructed on the domain of both uncertain parameters and optimization variables [68]. They assumed not only uncertain parameters but also optimization variables follow uniform distributions over the range of the search space and constructed the surrogate model with building blocks of the Legendre polynomials. All the listed surrogate models can provide the statistical moments via closed functions, which can make stochastic optimization feasible once the surrogate models are prepared in advance.

In this study, a surrogate model over the domain of both uncertain and design variables is applied to designing robust ORC for the first time. Prior to performing optimization, a simplified surrogate model, which is developed in this study, is constructed. The surrogate model has a structure of high order response surface (RS) model with

the coefficients of RS model expanded by PCE. By employing lasso regression, the constructed RS model can avoid the overfitting and have high accuracy in representing the relation between the design variables and the uncertainties [93]. The samples points for RS model are selected by Latin Hypercube [94]. The sample points required for constructing PCE model are collected by the sparse grids described in Chapter 3 Appendix. Evaluations of the original ORC model is carried out for the points collected by the sparse grids at every selected design variable. The surrogate model is constructed by the polynomial chaos spectral expansion of the coefficients for RS model. The coefficients of PCE model is obtained by the same method described in Chapter 3. The constructed surrogate model showed low enough cross validation error to use it for optimization.

4.2 Methodology

In this chapter, the description of ORC model, objective function, and constraints are omitted since they are the same in Chapter 3 except for the optimization algorithm. Once the surrogate model is constructed, Bayesian algorithm is no longer a good option for optimization because of the stochastic nature of the algorithm [85]. Since Bayesian algorithm may give difference optimum points at every attempt of optimization so it can not be sure that the ORC design is global optimum. Therefore, in this chapter, a non-derivative optimization algorithm called DIRECT is employed for efficiently solving the optimization problems considering the nonlinear nature of the developed model [95].

4.2.1 Construction of RS model

In this step, the uncertain variables are not considered as surrogate variables, therefore sampling is performed at a fixed uncertain variable vector and the design variable $u = \{\bar{x}, P_{pu}, P_{ex}\}$ is varied using Latin Hypercube method [94].

$$Y_{RS}^{(r)}(u)\Big|_{\Theta} = \left(\sum_{w=0}^{N_z-1} \beta_w^{(r)} z_w(u)\right)\Bigg|_{\Theta} \tag{4.2.1}$$

where $y_{(i)}^{RS}(u)\Big|_{\Theta}$ is the i^{th} realization of regressed RS model at a fixed uncertain vector Θ, which is composed of the varied critical temperature, critical pressure, composition, and heat source temperature. $\beta_w^{(r)}$ is the w^{th} element in the coefficient vector of the polynomial $y_{RS}^{(r)}(u)\Big|_{\Theta}$ and $z_w(u)$ is th w^{th} RS basis which can be expressed as

$$z_w(u) \in \{u_1, \ldots, u_{N_u}, u_1^2, u_1u_2, \ldots, u_{N_u}^{n_s}\} \cup \{1\} \tag{4.2.2}$$

where N_u and n_s are the dimension of design variables and the order of the polynomial, respectively. With N_S number of sampled data from the ORC model $\hat{Y}$, the coefficient vector $\beta^{(r)}$ can be obtained by LASSO regression.

$$\beta^{(r)} = \arg\min_{\beta^{(r)}} \left\{ \frac{1}{N_S} \sum_{i=1}^{N_S} (\hat{Y}(u^{(i)}, t) - Y_{RS}^{(r)}(u^{(i)}, t))^2 + \lambda_s ||\beta^{(r)}||_1 \right\} \tag{4.2.3}$$

The total number of the bases, N_z, is

$$N_z = \frac{(N_u + n_s)!}{N_u! n_s!} \tag{4.2.4}$$

In Eq. (4.2.3), l_1-regularization term $||\beta^{(r)}||_1$ is added to the squared error to allow for the sparse coefficient vector. The value of λ_S in Eq. (4.2.3) is determined by selecting

the number which gives the minimum cross validation error. Since $Y_{RS}^{(r)}(u)$ should be constructed as many as the sparse grids needs, N_{grid} number of $Y_{RS}^{(r)}(u)$ is required, which is determined Smolyak sparse grid quadrature [83].

4.2.2 Construction of RS-PC model

When $\boldsymbol{\xi}$ denotes the iso-transformed Θ, the truncated model output Y_{PC} by PCE is given by

$$Y_{PC} = \sum_{\boldsymbol{\alpha}\in\mathcal{A}} Y_{\boldsymbol{\alpha}}\Psi_{\boldsymbol{\alpha}}(\boldsymbol{\xi}) + \epsilon_{pc} \tag{4.2.5}$$

where $\Psi_{\boldsymbol{\alpha}}(\boldsymbol{\xi})$ is multivariate orthonormal polynomials induced by tensor product of univariate polynomials $\psi^{(j)}_{\alpha_j}(\boldsymbol{\xi}_j)$, i.e. $\Psi_{\boldsymbol{\alpha}}(\boldsymbol{\xi}) = \prod_{j=1}^{N_{\boldsymbol{\xi}}} \psi^{(j)}_{\alpha_j}(\boldsymbol{\xi}_j)$ such that $\mathbb{E}\left[\Psi_a\Psi_b\right] = \delta_{ab}$ (δ_{ab} is Kronecker delta). $Y_{\boldsymbol{\alpha}}$ is the coefficient vector for PCE. The univariate PC basis $\psi^{(j)}_{\alpha_j}(\boldsymbol{\xi}_j)$ should be selected as an orthonormal polynomial with respect to $f(\boldsymbol{\xi}_j)$. In case of uniformly distributed $\boldsymbol{\xi} \sim \mathbb{U}(-1, 1)$, the corresponding PC basis has to be Legendre polynomial [96]. $\boldsymbol{\alpha} = \{\boldsymbol{\alpha}_1, \ldots, \boldsymbol{\alpha}_{N_{\boldsymbol{\xi}}}\}$ are multi-indices and the set $\mathcal{A}$ is the truncated set of the indices. Since the PC model uses truncated indices for approximation of the original model, truncation error ϵ_{pc} is inevitable. The total number of polynomial basis terms for PCE, N_{pc}, is given by

$$N_{pc} = \frac{(N_{\boldsymbol{\xi}} + n_{pc})!}{N_{\boldsymbol{\xi}}! n_{pc}!} \tag{4.2.6}$$

where n_{pc} is the order of PC.

By expanding the coefficients of Eq. (4.2.1) as a function of $\boldsymbol{\xi}$ based on PC, the surrogate model can be expressed as

$$Y_{RS-PC}(u, \boldsymbol{\xi}) = \sum_{w=0}^{N_z-1} \boldsymbol{\beta}_w(\boldsymbol{\xi})\bar{z}_w(u) \tag{4.2.7}$$

where Y_{RS-PC} is the output value of the surrogate model. The coefficient vector $\boldsymbol{\beta}_w$

is approximated by PCE.

$$\boldsymbol{\beta}_w(\boldsymbol{\xi}) = \sum_{\boldsymbol{\alpha}\in A} \boldsymbol{Y}_{w,\boldsymbol{\alpha}} \Psi_{\boldsymbol{\alpha}}(\boldsymbol{\xi}) \tag{4.2.8}$$

$$\Psi_{\boldsymbol{\alpha}}(\boldsymbol{\xi}) = \prod_{j=1}^{N_{\boldsymbol{\xi}}} \psi_{\alpha_j}^{(j)}(\boldsymbol{\xi}_j) \qquad s.t. \qquad \mathbb{E}\left[\Psi_a \Psi_b\right] = \delta_{ab} \tag{4.2.9}$$

The coefficients of RS-PC model, $\boldsymbol{Y}_{w,\boldsymbol{\alpha}}$ can be obtained using a projection method called Galerkin method [97, 98].

$$\boldsymbol{Y}_{w,\boldsymbol{\alpha_k}} = \frac{<\beta_w(\boldsymbol{\xi}), \Psi_{\boldsymbol{\alpha_k}}(\boldsymbol{\xi})>}{<\Psi^2_{\boldsymbol{\alpha_k}}>} = \int_\Omega \beta_w(\boldsymbol{\xi}), \Psi_{\boldsymbol{\alpha_k}}(\boldsymbol{\xi}) f_{\boldsymbol{\xi}}(\boldsymbol{\xi}) d\boldsymbol{\xi} \tag{4.2.10}$$

where $\Omega \subset \mathbb{R}^{N_{\boldsymbol{\xi}}}$ is the range of ξ and $\boldsymbol{\alpha_k} \in \boldsymbol{\alpha}$. The right-hand side of Eq. (4.2.10) can be computed numerically using quadrature rule.

$$\int_\Omega \beta_w(\boldsymbol{\xi}), \Psi_{\boldsymbol{\alpha_k}}(\boldsymbol{\xi}) f_{\boldsymbol{\xi}}(\boldsymbol{\xi}) d\boldsymbol{\xi} \approx \sum_{v=1}^{N_{grid}} \beta_w(\boldsymbol{\xi}^{(v)}), \Psi_{\boldsymbol{\alpha_k}}(\boldsymbol{\xi}^{(v)}) f_{\boldsymbol{\xi}}(\boldsymbol{\xi}^{(v)}) \tag{4.2.11}$$

Since one coefficient of the RS model is regressed by N_{pc} bases, the total number of coefficients is $N_z \times N_{pc}$. Therefore, each coefficient requires N_{gird} number of sample points, and in total, $N_S \times N_{gird}$ samples should be collected to construct the surrogate model. The readers who wants to know details of the sparse grid quadrature rule may see Appendix in Chapter 3.

4.2.3 Postprocessing

Once the surrogate model is prepared, the approximate values for the mean and the variance can be computed analytically. The design variable u is fixed at a specific condition. Using the mean of Y_{RS-PC}, the variance is expressed as

$$\mathrm{Var}(Y_{RS-PC}) = \mathbb{E}[(Y_{RS-PC})^2] - \mathbb{E}[Y_{RS-PC}]^2 \tag{4.2.12}$$

where $\mathbb{E}[\cdot]$ is a mean with respect to $\boldsymbol{\xi}$. The mean value $\mathbb{E}[Y_{RS-PC}]$ in Eq. (4.2.12) can be calculated using Eq. (4.2.7) - (4.2.8).

$$\mathbb{E}[Y_{RS-PC}(u,\boldsymbol{\xi})] = \mathbb{E}\left[\sum_{w=0}^{N_z-1}\sum_{\boldsymbol{\alpha}\in A}\boldsymbol{Y}_{w,\boldsymbol{\alpha}}\Psi_{\boldsymbol{\alpha}}(\boldsymbol{\xi})z_w(u)\right] \tag{4.2.13}$$

$$= \mathbb{E}\left[\sum_{w=0}^{N_z-1}\boldsymbol{Y}_{w,0}z_w(u)\right] \tag{4.2.14}$$

In Eq. (4.2.14), except for the case of $\boldsymbol{\alpha}=0$, the PC basis $\Psi_{\boldsymbol{\alpha}}(\boldsymbol{\xi})$ and the corresponding coefficient $\boldsymbol{Y}_{w,\boldsymbol{\alpha}}$ are removed because $\Psi_{\boldsymbol{\alpha}}(\boldsymbol{\xi})$ is orthogonal to the probability density function of $\boldsymbol{\xi}$. Since Eq. (4.2.14) is irrelevant to $\boldsymbol{\xi}$, $\mathbb{E}[Y_{RS-PC}]$ becomes

$$\mathbb{E}[Y_{RS-PC}(u,\boldsymbol{\xi})] = \sum_{w=0}^{N_z-1}\boldsymbol{Y}_{w,0}z_w(u) \tag{4.2.15}$$

Likewise, $\mathbb{E}[(Y_{RS-PC})^2]$ can be derived using (4.2.7) - (4.2.8).

$$\mathbb{E}[(Y_{RS-PC}(u,\boldsymbol{\xi}))^2] = \mathbb{E}\left[\left(\sum_{w=0}^{N_z-1}\sum_{\boldsymbol{\alpha}\in\mathcal{A}}\boldsymbol{Y}_{w,\boldsymbol{\alpha}}\Psi_{\boldsymbol{\alpha}}(\boldsymbol{\xi})z_w(u)\right)^2\right] \tag{4.2.16}$$

$$= \mathbb{E}\left[\sum_{\boldsymbol{\alpha}\in\mathcal{A}}\left(\sum_{w=0}^{N_z-1}\boldsymbol{Y}_{w,\boldsymbol{\alpha}}\Psi_{\boldsymbol{\alpha}}(\boldsymbol{\xi})z_w(u)\right)^2\right] \tag{4.2.17}$$

$$= \mathbb{E}\left[\sum_{\boldsymbol{\alpha}\in\mathcal{A}}\Psi_{\boldsymbol{\alpha}}(\boldsymbol{\xi})^2\left(\sum_{w=0}^{N_z-1}\boldsymbol{Y}_{w,\boldsymbol{\alpha}}z_w(u)\right)^2\right] \tag{4.2.18}$$

By the orthogonality of the multivariate basis $\Psi_{\boldsymbol{\alpha}}$, terms associated with $\Psi_a \Psi_b$ such that $a \neq b$ becomes 0 in Eq. (4.2.16). $\Psi^2_{\boldsymbol{\alpha}}$ in Eq. (4.2.18) equals 1 therefore it is reduced to

$$\mathbb{E}[(Y_{RS-PC}(u,\boldsymbol{\xi}))^2] = \mathbb{E}\left[\sum_{\boldsymbol{\alpha}\in\mathcal{A}}\left(\sum_{w=0}^{N_z-1}\boldsymbol{Y}_{w,\boldsymbol{\alpha}} z_w(u)\right)^2\right] \tag{4.2.19}$$

Since Eq. (4.2.14) is irrelevant to $\boldsymbol{\xi}$, $\mathbb{E}[Y_{RS-PC}]$ becomes

$$\mathbb{E}[(Y_{RS-PC}(u,\boldsymbol{\xi}))^2] = \sum_{\boldsymbol{\alpha}\in\mathcal{A}}\left(\sum_{w=0}^{N_z-1}\boldsymbol{Y}_{w,\boldsymbol{\alpha}} z_w(u)\right)^2 \tag{4.2.20}$$

Inserting Eq. (4.2.15) and Eq. (4.2.20) to Eq. (4.2.12), the variance is given by

$$\text{Var}(Y_{RS-PC}(u,\boldsymbol{\xi})) = \sum_{\boldsymbol{\alpha}\in\mathcal{A}}\left(\sum_{w=0}^{N_z-1}\boldsymbol{Y}_{w,\boldsymbol{\alpha}} z_w(u)\right)^2 - \left(\sum_{w=0}^{N_z-1}\boldsymbol{Y}_{w,0} z_w(u)\right)^2 \tag{4.2.21}$$

If the redundant terms are removed in right-hand side of Eq. (4.2.21), the variance can be expressed as an explicit form of equation.

$$\text{Var}(Y_{RS-PC}(u,\boldsymbol{\xi})) = \sum_{\boldsymbol{\alpha}\in\mathcal{A}\setminus 0}\left(\sum_{w=0}^{N_z-1}\boldsymbol{Y}_{w,\boldsymbol{\alpha}} z_w(u)\right)^2 \tag{4.2.22}$$

Now that the statistical moments are derived from the surrogate model, the objective function Eq. (3.1) can be replaced by putting Eq. (4.2.15) and Eq. (4.2.22). If the surrogate model output, Y_{RS-PC}, approximates the ORC power output imposed with penalty, Y_{pa}, then the objective function becomes

$$J(u) = \mathbb{E}[Y_{pa}] - \kappa \text{Var}[Y_{pa}] \tag{4.2.23}$$

$$= \sum_{w=0}^{N_z-1}\boldsymbol{Y}_{w,0} z_w(u) - \kappa \sum_{\boldsymbol{\alpha}\in\mathcal{A}\setminus 0}\left(\sum_{w=0}^{N_z-1}\boldsymbol{Y}_{w,\boldsymbol{\alpha}} z_w(u)\right)^2 \tag{4.2.24}$$

In this study, the weight, κ, is fixed at 0.5 and the Pareto analysis will be remained for the future work.

4.3 Implementation

Implementation in this chapter is based on the result of Section 3.2.4 and uses the same ORC setting in Section 3.2. The working fluid combination, $wk4$, which is composed of R236fa, R23, and R14, since it turns out to be the most robust wokring fluid. The penalty parameters γ_1 and γ_2 are selected as 5 and 7 respectively according to the sensitivity analysis in Section 3.2.3. The uncertain variable vector is the collection of the composition, the temperature of heat source, the critical temperature of each component, and the critical pressure of each component in working fluid. Total 9 variables are considered as uncertain variables (the composition includes only 2 variables since a fraction of a component in the working fluid mixture is linearly dependent on other fractions as in Eq. (**??**)). The composition and the temperature of heat source are assumed to vary within the range of 10% bound centered at the nominal design point, $\bar{x}$ and $T_{source} = 66.7^{\circ}\mathrm{C}$. The critical temperature, T_c, and pressure, P_c, are obtained from National Institute of Standards and Technology (NIST) database, which is listed in Table 4.1 [99].

Table 4.1: Assumptions for uncertain variables and data for uncertain parameters

Variables or parameters	Uncertainty	Source
x	$\bar{x} \pm 0.1\bar{x}$	See Section3.2
T_{source}	$T_{source} \pm 0.1T_{source}$ (°C)	
T_c of R236fa	124.9200 ± 0.06 (°C)	[99]
T_c of R23	25.8536 ± 0.0204 (°C)	[99]
T_c of R14	-45.6146 ± 0.0278 (°C)	[99]
P_c of R236fa	32.1920 ± 0.0689 (bar)	[99]
P_c of R23	48.1620 ± 0.2235 (bar)	[99]
P_c of R14	37.4500 ± 0.3394 (bar)	[99]

The order of RS model and PCE model, n_z and n_{pc} are set to 4 for both of them, therefore, the number of coefficient for RS model, N_z, is 70 and the number of coefficient for PCE model, N_{pc} is 715. As the coefficients for the surrogate model, Y_{RS-PC}, are the expansion of every RS coefficients, the number of the RS-PC model coefficients is $50,050 = 70 \times 715$. Likewise, N_{grid} number of samples is required for every N_S samples. In this work, N_S is set to 300 and the level of sparse grids, q, is set to 5 so $N_{grid} = 1,177$. In sum, the total number of evaluated samples is $353,100 = 300 \times 1,177$, which is more than two times larger than the number of coefficients, $N_z \times N_{pc}$, so it is large enough number of samples to obtain a high accuracy surrogate model [81].

4.3.1 Surrogate model training

Simulations for sampling are carried out via ASPEN PLUS v10 and construction of the surrogate model is coded in MATLAB 2018b. The verification result is presented in Fig. 4.1. The '+' markers stand for data points from Y_{RS-PC} and Y_{pa} at the same u and Θ. Although some deviations of Y_{RS-PC} from the original ORC model value are observed in Fig. 4.1, the overall trends of Y_{RS-PC} are coincident with those of Y_{pa}. A few samples of Y_{RS-PC} show relatively large deviation from Y_{pa} but it can be canceled out when the statistical moments are computed from the surrogate model. Therefore, a verification analysis for the mean and the variance should be performed. The mean square error (MSE) for the trained surrogate model was 0.1268.

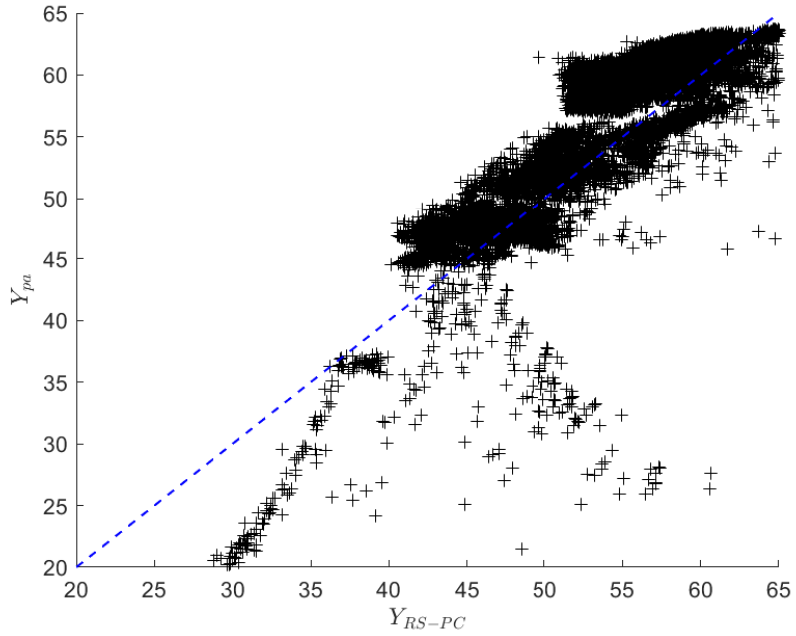

Figure 4.1: Comparison of surrogate model output with ORC model output.

The MSE for the mean and the variance were 0.0041 and 0.01, respectively, which much lower than MSE for Y_{RS-PC}. The trend for $\mathbb{E}[Y_{RS-PC}]$ coincides with $\mathbb{E}[Y_{pa}]$ but one for $Var[Y_{RS-PC}]$ does not match with $Var[Y_{pa}]$. However, $Var[Y_{pa}]$ mostly increases as $Var[Y_{RS-PC}]$ increases, and since $Var[Y_{RS-PC}]$ and $Var[Y_{pa}]$ have little influence on the objective function due to their small value compared to $\mathbb{E}[Y_{RS-PC}]$, the surrogate model can be used for optimization in spite of the regression error. To achieve the more accurate surrogate model, the order of RS and PCE should be raised, which inevitably requires higher level of sparse girds and larger amount of data.

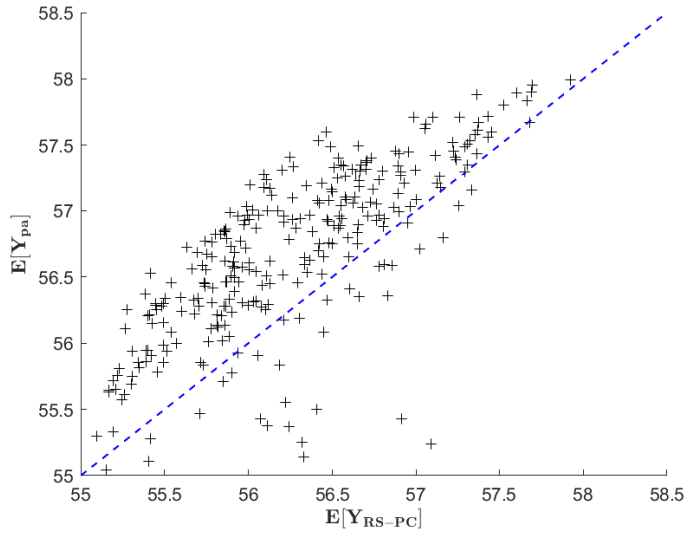

(a) Comparison of $\mathbb{E}(Y_{RS-PC})$ with $\mathbb{E}(Y_{pa})$

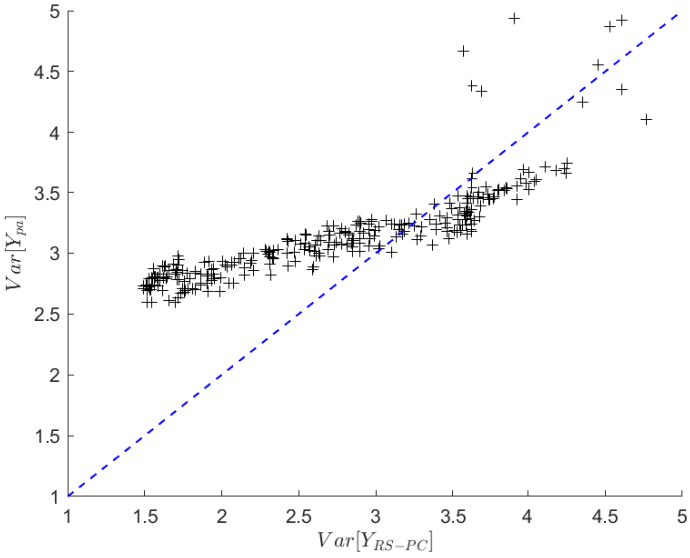

(b) Comparison of $Var(Y_{RS-PC})$ with $Var(Y_{pa})$

Figure 4.2: Statistical moments comparison for surrogate model and ORC model

4.3.2 Result

Using the prepared surrogate model, optimization for robust ORC design was carried out. The result is compared to the one from Chapter 3, that is, ORC design considering all the uncertainties listed in Table 4.1 is compared to ORC design considering only the uncertainty in the composition and ORC design without considering any uncertainty. The results are summarized in Table 4.2 and Fig. 4.3.

Table 4.2: Working fluid design result

Case	Constituent materials	Uncertainty	Y_{net} (MW)	$\mathbb{E}[Y_{pa}]$	$x = (x_1, x_2, x_3)$	P_{pu} (bar)	P_{ex} (bar)
Case 1		None	63.26	50.88	(0.2166, 0.7498, 0.0337)	24.84	0.78
Case 2	R236fa, R23, R14	$\bar{x} \pm 0.1\bar{x}$	54.95	45.33	(0.6892, 0.2878, 0.0230)	8.23	0.25
Case 3		All in Table 4.1	61.16	55.40	(0.1560, 0.6650, 0.1560)	28.00	1.11

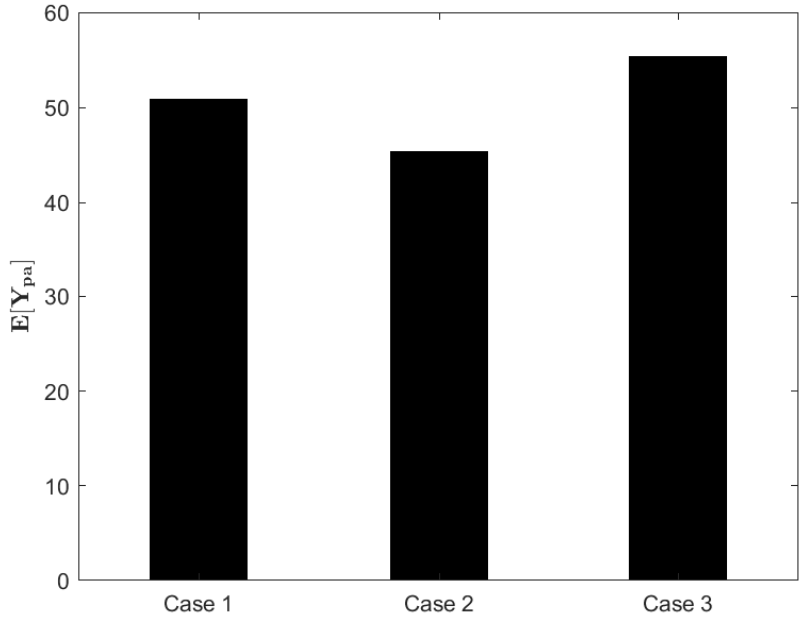

Figure 4.3: Comparison result of $\mathbb{E}[Y_{pa}]$.

In Table 4.2 and Fig. 4.3, Case 1, Case 2, and Case 3 mean the ORC design cases that consider no uncertainty, the varying composition, and all the uncertainties listed in Table 4.1. Y_{net} is evaluated at the nominal design point with assuming that the uncertainties in the thermodynamic parameters do not exist. The comparison result clearly demonstrates the need for the proposed methodology in designing ORCs. Except for Case 3, the values of Y_{net} are reduced by around 10 (MW) compared to $\mathbb{E}[Y_{pa}]$, which means that Case 1 and Case 2 are not likely to produce stable power output, or that the probabilities for occurrence of factors that may impede normal operation such as formation of liquid droplet in the expander and temperature crossover in the condenser. That is, the ORC designs of Case 1 and Case 2 are not robust compared to that of Case 3. Although the measure of robustness, $Y_net - \mathbb{E}[Y_{pa}]$, is slightly lower in Case 2 than Case 1, which implies Case 2 can produce power more consistently than Case 1 $\mathbb{E}[Y_{pa}]$ value for Case 2 is even smaller than one for Case 1. This result indicates the necessity of considering uncertainties existing in the parameters for the property model as well as for the composition. Case 2 is the result of being designed to avoid risks only from the uncertainty of composition, and in consequence, it becomes vulnerable to the risks from other uncertainties. The uncertainties listed in Table 4.1 should not be neglected to obtain the genuinely robust ORC design.

Fig. 4.4 - 4.6 represents robustness analysis of the design ORC. To observe variation of Y_{net}, Fig 4.4 shows the distribution of Y_{net}, where the loss of Y_{net} as a cost to obtain robustness can be checked. The distribution of $l - f_l$ is shown in Fig. 4.5. The

difference between $1 - f_l$ value and one means the amount of liquid droplet formation, so it can be seen as a measure of sensitivity for designed ORC. The distribution of ΔT_{vi}, which indicates the violation of the reference minimum temperature difference in the condenser, is represented in Fig. 4.6. Since ΔT_{vi} has a non-zero value only if its value is less than ΔT_{min}^{ref} (5 $^\circ$ C in this study), ΔT_{vi} can be used as a measure of the risk that the temperature crossover in the condenser occurs.

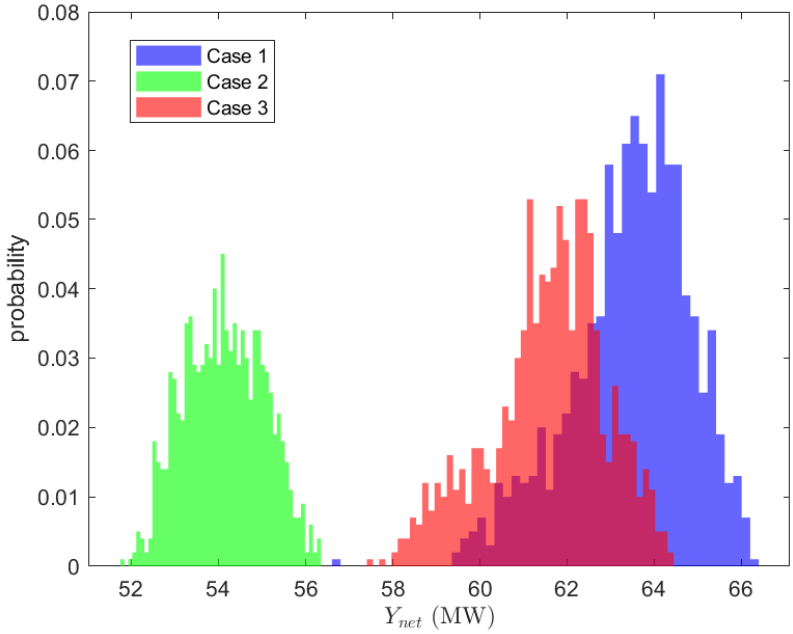

Figure 4.4: Y_{net} distribution from MC simulation.

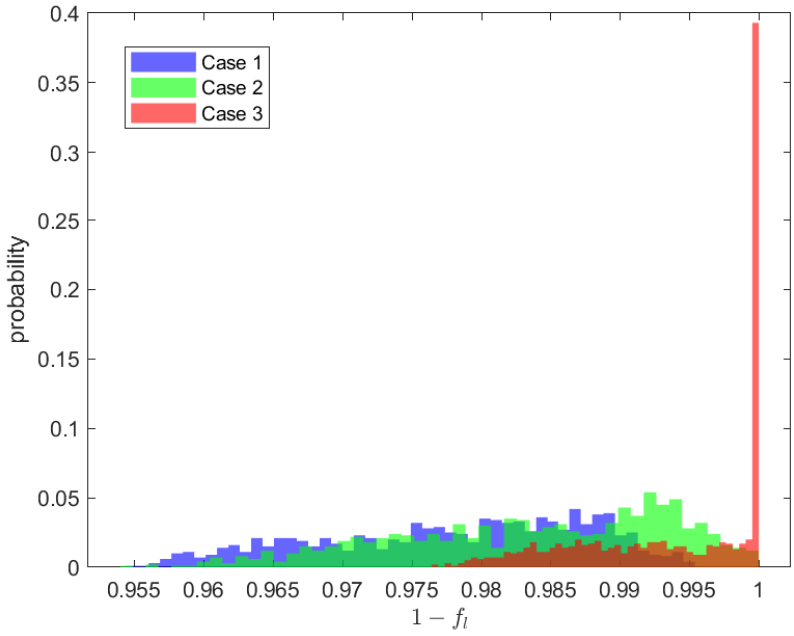

Figure 4.5: $1 - f_l$ distribution from MC simulation.

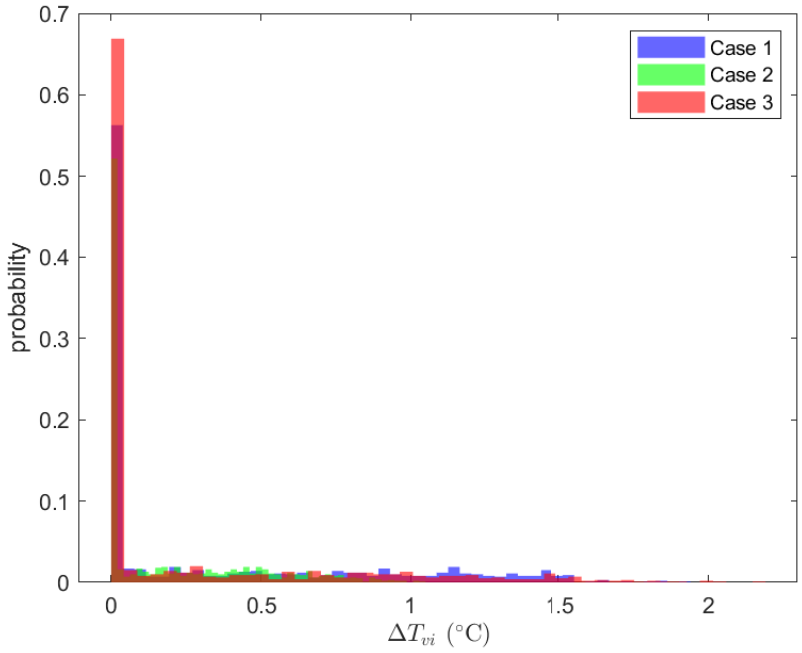

Figure 4.6: ΔT_{vi} distribution from MC simulation.

The color blue, green, and red stand for Case 1, Case 2, and Case 3, respectively. Y_{net} value for Case 3 is distributed between the values for Case 1 and Case 2, meaning that Case 3 costs relatively small reduction in the net power output compared to Case 1 to achieve robustness. Although Y_{net} for Case 3 is marginally shifted from Y_{net} for Case 1, $1 - f_l$ values for Case 3 is mostly distributed close to one. This can conclude the proposed method in this Chapter can design an ORC robust against the risk of formation of liquid droplet in the condenser. All the three cases show high probability for $\Delta T_{vi} = 0$. Therefore, the risk from the temperature crossover is less threatening than the formation of liquid droplet for all the optimal design cases. But still, Case 3 represents the probability higher than 0.65 for $\Delta T_{vi} = 0$, meaning that, regardless of the heat source and the composition varying during operation of ORC, and of the thermodynamic parameters different from the known values, Case 3 ORC design does not violate the soft constraint for the minimum temperature difference.

Meanwhile, Case 2, designed with considering only the uncertainty in the working fluid mixture composition, shows more robust against the risk associated with $1 - f_l$ than Case 1. However, Y_{net} values for Case 2 are distributed over much lower area than Case 3 values. Therefore, Case 2 is more robust than ORC design without consideration on the uncertainties, but failed to achieve high thermal efficiency. This leads to a conclusion that designing a robust and highly efficient ORC requires to consider uncertainties in both operating variables and thermodynamic parameters.

4.4 Conclusion

An optimization method using a surrogate model constructed over the domain of both uncertain and design variables is applied to designing robust ORC. Prior to performing optimization, a simplified surrogate model is constructed. The surrogate model has a structure of high order RS model with the coefficients of RS model expanded by PCE. By employing lasso regression, the constructed RS model can avoid the overfitting and have high accuracy in representing the relation between the design variables and the uncertainties [93]. The samples points for RS model are selected by Latin Hypercube [94]. The sample points required for constructing PCE model are collected by the sparse grids described in Chapter 3 Appendix. Evaluations of the original ORC model is carried out for the points collected by the sparse grids at every selected design variable. The surrogate model is constructed by the polynomial chaos spectral expansion of the coefficients for RS model. The constructed surrogate model showed low enough cross validation error to use it for optimization.

As a result of optimization, the newly found optimal ORC design shows stable performance compared to the optimal designs obtained in previous chapter when the operating condition varies from its nominal condition or the knowledge of the thermodynamic property model is incomplete. The comparison analysis proves the necessity for consideration on the uncertainties in both operating variables and thermodynamic parameters.

Chapter 5

Concluding remarks

A systematic method to design a robust ORC using LNG and multicomponent working fluid, which yields maximum power output even when the composition of the working fluid varies from the nominal point during operation of ORC has been developed. The proposed method seeks the optimal composition giving both the maximum mean and the minimum variance of ORC power output. To suppress the factors that adversely affect the operation of ORC (violation of minimum temperature difference in heat exchanger and formation of liquid droplet in expander), the objective function is penalized when they occur. The procedure to derive the statistical moments consists of two steps. Initially, the required heat exchanger area is obtained by simulation of ORC model with a nominal operating conditions (composition, pump discharge pressure, and expander discharge pressure). At the next step, the simulation is carried out again with the obtained area and the varying composition. The mass fraction of each substance in the working fluid is assumed to follow uniform distribution centered at the

nominal point. To obtain the mean and variance with a small number of simulations, PCE with sparse grid quadrature is employed. It has been shown that small changes in composition can have serious consequences for stable operation of ORC, and the design of working fluid by the proposed method allows flexible ORC operation despite the existence of uncertainty in the composition.

The optimization takes into account uncertainties in thermodynamic parameters and heat source. Using the selected working fluid which was turned out to be the most insensitive from the uncertainty of composition, optimization is carried out again for the case that the critical temperature and pressure of each substance composing the working fluid varies within its measurement uncertainty, which can be found in the literatures. Also, the temperature of the heat source varies from the nominal design point to enhance the operational flexibility of ORC. In sum, the design of ORC was performed assuming a total of the nine parameters or design variables with uncertainty, which requires excessive amount of computation with the method previously suggested. Therefore, the optimization using a surrogate model was devised to efficiently find the optimal and robust ORC design. Because the proposed surrogate model is constructed based on PCE, the statistical moments can be derived analytically, which leads to reduce the time for optimization drastically. ORC design using the surrogate model showed the highest output even when the parameters and design variables were changing from the nominal point.

The future work required to further refine the methodology proposed in this work

can be classified as two works: First of all, an efficient way to construct the surrogate model having higher accuracy in predicting the behavior of ORC output. Although the proposed surrogate model shows enough accuracy to be used for optimization, the surrogate model can be further improved even when more uncertainties are considered. This can be addressed by PCE model with the high PCE order, involving calculation of numerous samples of the original ORC model. Second of all, the target configuration of ORC model should be updated referring to recent developments of ORCs. The ORC model used in this study has the simplest configuration for its ease of discussion about robust design. The units commonly used to improve the efficiency of ORCs such as a recuperation unit and a super heater, should also be included in ORC configuration in order for the proposed method to be generally used in designing ORC.

Bibliography

[1] U. Lee, K. Kim, and C. Han, "Design and optimization of multi-component organic rankine cycle using liquefied natural gas cryogenic exergy," *Energy*, vol. 77, pp. 520–532, 2014.

[2] K. Kim, U. Lee, C. Kim, and C. Han, "Design and optimization of cascade organic rankine cycle for recovering cryogenic energy from liquefied natural gas using binary working fluid," *Energy*, vol. 88, pp. 304–313, 2015.

[3] Y. Liu and K. Guo, "A novel cryogenic power cycle for lng cold energy recovery," *Energy*, vol. 36, no. 5, pp. 2828–2833, 2011.

[4] H. Sun, H. Zhu, F. Liu, and H. Ding, "Simulation and optimization of a novel rankine power cycle for recovering cold energy from liquefied natural gas using a mixed working fluid," *Energy*, vol. 70, pp. 317–324, 2014.

[5] M. Z. Stijepovic, P. Linke, A. I. Papadopoulos, and A. S. Grujic, "On the role of working fluid properties in organic rankine cycle performance," *Applied Thermal Engineering*, vol. 36, pp. 406–413, 2012.

[6] P. Linke, A. Papadopoulos, and P. Seferlis, "Systematic methods for working fluid selection and the design, integration and control of organic rankine cycles—a review," *Energies*, vol. 8, no. 6, pp. 4755–4801, 2015.

[7] D. P. Molina-Thierry and A. Flores-Tlacuahuac, "Simultaneous optimal design of organic mixtures and rankine cycles for low-temperature energy recovery," *Industrial & Engineering Chemistry Research*, vol. 54, no. 13, pp. 3367–3383, 2015.

[8] H. Chen, D. Y. Goswami, and E. K. Stefanakos, "A review of thermodynamic cycles and working fluids for the conversion of low-grade heat," *Renewable and sustainable energy reviews*, vol. 14, no. 9, pp. 3059–3067, 2010.

[9] X. Shi and D. Che, "A combined power cycle utilizing low-temperature waste heat and lng cold energy," *Energy conversion and management*, vol. 50, no. 3, pp. 567–575, 2009.

[10] N. Zhang and N. Lior, "A novel near-zero co2 emission thermal cycle with lng cryogenic exergy utilization," *Energy*, vol. 31, no. 10-11, pp. 1666–1679, 2006.

[11] J. Wang, Z. Yan, M. Wang, and Y. Dai, "Thermodynamic analysis and optimization of an ammonia-water power system with lng (liquefied natural gas) as its heat sink," *Energy*, vol. 50, pp. 513–522, 2013.

[12] M. R. Gómez, R. F. Garcia, J. R. Gómez, and J. C. Carril, "Thermodynamic analysis of a brayton cycle and rankine cycle arranged in series exploiting the cold exergy of lng (liquefied natural gas)," *Energy*, vol. 66, pp. 927–937, 2014.

[13] I.-H. Choi, S. Lee, Y. Seo, and D. Chang, "Analysis and optimization of cascade rankine cycle for liquefied natural gas cold energy recovery," *Energy*, vol. 61, pp. 179–195, 2013.

[14] U. Lee, K. Park, Y. S. Jeong, S. Lee, and C. Han, "Design and analysis of a combined rankine cycle for waste heat recovery of a coal power plant using lng cryogenic exergy," *Industrial & Engineering Chemistry Research*, vol. 53, no. 23, pp. 9812–9824, 2014.

[15] F. Heberle, M. Preißinger, and D. Brüggemann, "Zeotropic mixtures as working fluids in organic rankine cycles for low-enthalpy geothermal resources," *Renewable Energy*, vol. 37, no. 1, pp. 364–370, 2012.

[16] G. Angelino and P. C. Di Paliano, "Multicomponent working fluids for organic rankine cycles (orcs)," *Energy*, vol. 23, no. 6, pp. 449–463, 1998.

[17] C. Carcasci, R. Ferraro, and E. Miliotti, "Thermodynamic analysis of an organic rankine cycle for waste heat recovery from gas turbines," *Energy*, vol. 65, pp. 91–100, 2014.

[18] F. Cataldo, R. Mastrullo, A. W. Mauro, and G. P. Vanoli, "Fluid selection of organic rankine cycle for low-temperature waste heat recovery based on thermal optimization," *Energy*, vol. 72, pp. 159–167, 2014.

[19] A. M. Delgado-Torres and L. García-Rodríguez, "Analysis and optimization of the low-temperature solar organic rankine cycle (orc)," *Energy conversion and Management*, vol. 51, no. 12, pp. 2846–2856, 2010.

[20] B.-T. Liu, K.-H. Chien, and C.-C. Wang, "Effect of working fluids on organic rankine cycle for waste heat recovery," *Energy*, vol. 29, no. 8, pp. 1207–1217, 2004.

[21] H. M. Hettiarachchi, M. Golubovic, W. M. Worek, and Y. Ikegami, "Optimum design criteria for an organic rankine cycle using low-temperature geothermal heat sources," *Energy*, vol. 32, no. 9, pp. 1698–1706, 2007.

[22] V. Maizza and A. Maizza, "Unconventional working fluids in organic rankine-cycles for waste energy recovery systems," *Applied thermal engineering*, vol. 21, no. 3, pp. 381–390, 2001.

[23] D. Meinel, C. Wieland, and H. Spliethoff, "Effect and comparison of different working fluids on a two-stage organic rankine cycle (orc) concept," *Applied Thermal Engineering*, vol. 63, no. 1, pp. 246–253, 2014.

[24] A. I. Papadopoulos, M. Stijepovic, and P. Linke, "On the systematic design and selection of optimal working fluids for organic rankine cycles," *Applied thermal engineering*, vol. 30, no. 6-7, pp. 760–769, 2010.

[25] R. Rayegan and Y. Tao, "A procedure to select working fluids for solar organic rankine cycles (orcs)," *Renewable Energy*, vol. 36, no. 2, pp. 659–670, 2011.

[26] B. Saleh, G. Koglbauer, M. Wendland, and J. Fischer, "Working fluids for low-temperature organic rankine cycles," *Energy*, vol. 32, no. 7, pp. 1210–1221, 2007.

[27] A. Schuster, S. Karellas, and R. Aumann, "Efficiency optimization potential in supercritical organic rankine cycles," *Energy*, vol. 35, no. 2, pp. 1033–1039, 2010.

[28] Z. Shengjun, W. Huaixin, and G. Tao, "Performance comparison and parametric optimization of subcritical organic rankine cycle (orc) and transcritical power cycle system for low-temperature geothermal power generation," *Applied energy*, vol. 88, no. 8, pp. 2740–2754, 2011.

[29] E. Wang, H. Zhang, B. Fan, M. Ouyang, Y. Zhao, and Q. Mu, "Study of working fluid selection of organic rankine cycle (orc) for engine waste heat recovery," *Energy*, vol. 36, no. 5, pp. 3406–3418, 2011.

[30] R.-J. Xu and Y.-L. He, "A vapor injector-based novel regenerative organic rankine cycle," *Applied Thermal Engineering*, vol. 31, no. 6-7, pp. 1238–1243, 2011.

[31] V. Lemort, S. Quoilin, C. Cuevas, and J. Lebrun, "Testing and modeling a scroll expander integrated into an organic rankine cycle," *Applied Thermal Engineering*, vol. 29, no. 14-15, pp. 3094–3102, 2009.

[32] C. Zamfirescu and I. Dincer, "Thermodynamic analysis of a novel ammonia–water trilateral rankine cycle," *Thermochimica Acta*, vol. 477, no. 1-2, pp. 7–15, 2008.

[33] C.-L. Chen, F.-Y. Chang, T.-H. Chao, H.-C. Chen, and J.-Y. Lee, "Heat-exchanger network synthesis involving organic rankine cycle for waste heat recovery," *Industrial & Engineering Chemistry Research*, vol. 53, no. 44, pp. 16924–16936, 2014.

[34] M. Z. Stijepovic, A. I. Papadopoulos, P. Linke, A. S. Grujic, and P. Seferlis, "An exergy composite curves approach for the design of optimum multi-pressure organic rankine cycle processes," *Energy*, vol. 69, pp. 285–298, 2014.

[35] J. Sun and W. Li, "Operation optimization of an organic rankine cycle (orc) heat recovery power plant," *Applied Thermal Engineering*, vol. 31, no. 11-12, pp. 2032–2041, 2011.

[36] D.-Y. Peng and D. B. Robinson, "A new two-constant equation of state," *Industrial & Engineering Chemistry Fundamentals*, vol. 15, no. 1, pp. 59–64, 1976.

[37] K. Satanphol, W. Pridasawas, and B. Suphanit, "A study on optimal composition of zeotropic working fluid in an organic rankine cycle (orc) for low grade heat recovery," *Energy*, vol. 123, pp. 326–339, 2017.

[38] P. Mavrou, A. I. Papadopoulos, M. Z. Stijepovic, P. Seferlis, P. Linke, and S. Voutetakis, "Novel and conventional working fluid mixtures for solar rankine cycles: Performance assessment and multi-criteria selection," *Applied Thermal Engineering*, vol. 75, pp. 384 – 396, 2015.

[39] V. L. Le, M. Feidt, A. Kheiri, and S. Pelloux-Prayer, "Performance optimization of low-temperature power generation by supercritical orcs (organic rankine cycles) using low gwp (global warming potential) working fluids," *Energy*, vol. 67, pp. 513 – 526, 2014.

[40] J. Hærvig, K. Sørensen, and T. J. Condra, "Guidelines for optimal selection of working fluid for an organic rankine cycle in relation to waste heat recovery," *Energy*, vol. 96, pp. 592–602, 2016.

[41] U. Lee and A. Mitsos, "Optimal multicomponent working fluid of organic rankine cycle for exergy transfer from liquefied natural gas regasification," *Energy*, vol. 127, pp. 489–501, 2017.

[42] A. I. Papadopoulos, M. Stijepovic, P. Linke, P. Seferlis, and S. Voutetakis, "Toward optimum working fluid mixtures for organic rankine cycles using molecular

design and sensitivity analysis," *Industrial & Engineering Chemistry Research*, vol. 52, no. 34, pp. 12116–12133, 2013.

[43] N. V. Sahinidis, "Baron: A general purpose global optimization software package," *Journal of global optimization*, vol. 8, no. 2, pp. 201–205, 1996.

[44] J. Frutiger, J. Andreasen, W. Liu, H. Spliethoff, F. Haglind, J. Abildskov, and G. Sin, "Working fluid selection for organic rankine cycles–impact of uncertainty of fluid properties," *Energy*, vol. 109, pp. 987–997, 2016.

[45] P. Mavrou, A. I. Papadopoulos, P. Seferlis, P. Linke, and S. Voutetakis, "Selection of working fluid mixtures for flexible organic rankine cycles under operating variability through a systematic nonlinear sensitivity analysis approach," *Applied Thermal Engineering*, vol. 89, pp. 1054–1067, 2015.

[46] E. A. Bufi, S. M. Camporeale, and P. Cinnella, "Robust optimization of an organic rankine cycle for heavy duty engine waste heat recovery," *Energy Procedia*, vol. 129, pp. 66–73, 2017.

[47] M. M. Santos-Rodriguez, A. Flores-Tlacuahuac, and V. M. Zavala, "A stochastic optimization approach for the design of organic fluid mixtures for low-temperature heat recovery," *Applied energy*, vol. 198, pp. 145–159, 2017.

[48] M. Pasetti, C. M. Invernizzi, and P. Iora, "Thermal stability of working fluids for organic rankine cycles: An improved survey method and experimental results for

cyclopentane, isopentane and n-butane," *Applied Thermal Engineering*, vol. 73, no. 1, pp. 764–774, 2014.

[49] H. Kruse and F. Rinne, "Performance and leakage investigations of refrigeration and airconditioning systems using refrigerant mixtures as working fluids," *International Refrigeration and Air Conditioning Conference*, pp. 621–630, 1992.

[50] P. Glaser, M. Schick, K. Petridis, and V. Heuveline, "Comparison between a polynomial chaos surrogate model and markov chain monte carlo for inverse uncertainty quantification based on an electric drive test bench," in *ECCOMAS Congress*, pp. 8809–8826, 2016.

[51] A. Kaintura, T. Dhaene, and D. Spina, "Review of polynomial chaos-based methods for uncertainty quantification in modern integrated circuits," *Electronics*, vol. 7, no. 3, p. 30, 2018.

[52] R. Field Jr and M. Grigoriu, "On the accuracy of the polynomial chaos approximation," *Probabilistic Engineering Mechanics*, vol. 19, no. 1-2, pp. 65–80, 2004.

[53] T. Crestaux, O. Le Maı^tre, and J.-M. Martinez, "Polynomial chaos expansion for sensitivity analysis," *Reliability Engineering & System Safety*, vol. 94, no. 7, pp. 1161–1172, 2009.

[54] D. Xiu and G. E. Karniadakis, "The wiener–askey polynomial chaos for stochastic differential equations," *SIAM journal on scientific computing*, vol. 24, no. 2, pp. 619–644, 2002.

[55] H. N. Najm, "Uncertainty quantification and polynomial chaos techniques in computational fluid dynamics," *Annual review of fluid mechanics*, vol. 41, pp. 35–52, 2009.

[56] Y. Zhang and N. V. Sahinidis, "Uncertainty quantification in co2 sequestration using surrogate models from polynomial chaos expansion," *Industrial & Engineering Chemistry Research*, vol. 52, no. 9, pp. 3121–3132, 2012.

[57] M. Villegas, F. Augustin, A. Gilg, A. Hmaidi, and U. Wever, "Application of the polynomial chaos expansion to the simulation of chemical reactors with uncertainties," *Mathematics and Computers in Simulation*, vol. 82, no. 5, pp. 805–817, 2012.

[58] D. Xiu and G. E. Karniadakis, "Modeling uncertainty in flow simulations via generalized polynomial chaos," *Journal of computational physics*, vol. 187, no. 1, pp. 137–167, 2003.

[59] B. Sudret, "Global sensitivity analysis using polynomial chaos expansions," *Reliability engineering & system safety*, vol. 93, no. 7, pp. 964–979, 2008.

[60] O. Garcia-Cabrejo and A. Valocchi, "Global sensitivity analysis for multivariate output using polynomial chaos expansion," *Reliability Engineering & System Safety*, vol. 126, pp. 25–36, 2014.

[61] L. Formaggia, A. Guadagnini, I. Imperiali, V. Lever, G. Porta, M. Riva, A. Scotti, and L. Tamellini, "Global sensitivity analysis through polynomial chaos ex-

pansion of a basin-scale geochemical compaction model," *Computational Geosciences*, vol. 17, no. 1, pp. 25–42, 2013.

[62] E. H. Sandoval, F. Anstett-Collin, and M. Basset, "Sensitivity study of dynamic systems using polynomial chaos," *Reliability Engineering & System Safety*, vol. 104, pp. 15–26, 2012.

[63] M. Dodson and G. T. Parks, "Robust aerodynamic design optimization using polynomial chaos," *Journal of Aircraft*, vol. 46, no. 2, pp. 635–646, 2009.

[64] N. H. Kim, H. Wang, and N. V. Queipo, "Efficient shape optimization under uncertainty using polynomial chaos expansions and local sensitivities," *AIAA journal*, vol. 44, no. 5, pp. 1112–1116, 2006.

[65] D. Wei, Z. Cui, and J. Chen, "Robust optimization based on a polynomial expansion of chaos constructed with integration point rules," *Proceedings of the Institution of Mechanical Engineers, Part C: Journal of Mechanical Engineering Science*, vol. 223, no. 5, pp. 1263–1272, 2009.

[66] F. Xiong, B. Xue, Z. Yan, and S. Yang, "Polynomial chaos expansion based robust design optimization," in *Quality, Reliability, Risk, Maintenance, and Safety Engineering (ICQR2MSE), 2011 International Conference on*, pp. 868–873, IEEE, 2011.

[67] A. Ruderman, S.-K. Choi, J. Patel, A. Kumar, and J. K. Allen, "Simulation-based robust design of multiscale products," *Journal of Mechanical Design*, vol. 132, no. 10, p. 101003, 2010.

[68] D. E. Shen and R. D. Braatz, "Polynomial chaos-based robust design of systems with probabilistic uncertainties," *AIChE Journal*, vol. 62, no. 9, pp. 3310–3318, 2016.

[69] S. Poles and A. Lovison, "A polynomial chaos approach to robust multiobjective optimization," in *Dagstuhl Seminar Proceedings*, Schloss Dagstuhl-Leibniz-Zentrum für Informatik, 2009.

[70] J. Villadsen and M. L. Michelsen, *Solution of differential equation models by polynomial approximation*. Prentice-Hall, 1978.

[71] T. J. Sullivan, *Introduction to uncertainty quantification*, vol. 63. Springer, 2015.

[72] B. Ganapathysubramanian and N. Zabaras, "Sparse grid collocation schemes for stochastic natural convection problems," *Journal of Computational Physics*, vol. 225, no. 1, pp. 652–685, 2007.

[73] H. Zhu, X. Zeng, W. Cai, J. Xue, and D. Zhou, "A sparse grid based spectral stochastic collocation method for variations-aware capacitance extraction of interconnects under nanometer process technology," in *Proceedings of the conference on Design, automation and test in Europe*, pp. 1514–1519, EDA Consortium, 2007.

[74] G. Lin and A. M. Tartakovsky, "An efficient, high-order probabilistic collocation method on sparse grids for three-dimensional flow and solute transport in randomly heterogeneous porous media," *Advances in Water Resources*, vol. 32, no. 5, pp. 712–722, 2009.

[75] C. W. Clenshaw and A. R. Curtis, "A method for numerical integration on an automatic computer," *Numerische Mathematik*, vol. 2, no. 1, pp. 197–205, 1960.

[76] M. Eldred and J. Burkardt, "Comparison of non-intrusive polynomial chaos and stochastic collocation methods for uncertainty quantification," in *47th AIAA aerospace sciences meeting including the new horizons forum and aerospace exposition*, p. 976, 2009.

[77] D. Xiu, *Numerical methods for stochastic computations: a spectral method approach*. Princeton university press, 2010.

[78] B. Sudret and A. Der Kiureghian, *Stochastic finite element methods and reliability: a state-of-the-art report*. Department of Civil and Environmental Engineering, University of California Berkeley, 2000.

[79] J. Pacheco and H. A. Kidd, "Assessing liquid droplet erosion potential in centrifugal compressor impellers," *Proceedings of the 38th Turbomachinery Symposium*, pp. 123–128, 2009.

[80] R. C. Smith, *Uncertainty quantification: theory, implementation, and applications*, vol. 12. Siam, 2013.

[81] J. Hampton and A. Doostan, "Coherence motivated sampling and convergence analysis of least squares polynomial chaos regression," *Computer Methods in Applied Mechanics and Engineering*, vol. 290, pp. 73–97, 2015.

[82] M. Stoyanov, "Hierarchy-direction selective approach for locally adaptive sparse grids," *Oak Ridge National Laboratory, Tennessee*, 2013.

[83] M. K. Stoyanov and C. G. Webster, "A dynamically adaptive sparse grids method for quasi-optimal interpolation of multidimensional functions," *Computers & Mathematics with Applications*, vol. 71, no. 11, pp. 2449–2465, 2016.

[84] D. B. Robinson, D.-Y. Peng, and S. Y. Chung, "The development of the peng-robinson equation and its application to phase equilibrium in a system containing methanol," *Fluid Phase Equilibria*, vol. 24, no. 1-2, pp. 25–41, 1985.

[85] M. A. Gelbart, J. Snoek, and R. P. Adams, "Bayesian optimization with unknown constraints," *arXiv preprint arXiv:1403.5607*, 2014.

[86] V. Barthelmann, E. Novak, and K. Ritter, "High dimensional polynomial interpolation on sparse grids," *Advances in Computational Mathematics*, vol. 12, no. 4, pp. 273–288, 2000.

[87] T. Gerstner and M. Griebel, "Numerical integration using sparse grids," *Numerical algorithms*, vol. 18, no. 3-4, p. 209, 1998.

[88] D. Xiu and J. S. Hesthaven, "High-order collocation methods for differential equations with random inputs," *SIAM Journal on Scientific Computing*, vol. 27, no. 3, pp. 1118–1139, 2005.

[89] N. V. Queipo, R. T. Haftka, W. Shyy, T. Goel, R. Vaidyanathan, and P. K. Tucker, "Surrogate-based analysis and optimization," *Progress in aerospace sciences*, vol. 41, no. 1, pp. 1–28, 2005.

[90] A. I. Forrester and A. J. Keane, "Recent advances in surrogate-based optimization," *Progress in aerospace sciences*, vol. 45, no. 1-3, pp. 50–79, 2009.

[91] R. Schobi, B. Sudret, and J. Wiart, "Polynomial-chaos-based kriging," *International Journal for Uncertainty Quantification*, vol. 5, no. 2, 2015.

[92] C. Mai, M. Spiridonakos, E. Chatzi, and B. Sudret, "Surrogate modelling for stochastic dynamical systems by combining narx models and polynomial chaos expansions," *arXiv preprint arXiv:1604.07627*, 2016.

[93] R. Tibshirani, "Regression shrinkage and selection via the lasso," *Journal of the Royal Statistical Society. Series B (Methodological)*, pp. 267–288, 1996.

[94] B. Minasny and A. B. McBratney, "A conditioned latin hypercube method for sampling in the presence of ancillary information," *Computers & geosciences*, vol. 32, no. 9, pp. 1378–1388, 2006.

[95] D. E. Finkel, "Direct optimization algorithm user guide," *Center for Research in Scientific Computation, North Carolina State University*, vol. 2, 2003.

[96] M. Abramowitz and I. A. Stegun, *Handbook of mathematical functions: with formulas, graphs, and mathematical tables*, vol. 55. Courier Corporation, 1964.

[97] J. Beck, F. Nobile, L. Tamellini, and R. Tempone, "Convergence of quasi-optimal stochastic galerkin methods for a class of pdes with random coefficients," *Computers & Mathematics with Applications*, vol. 67, no. 4, pp. 732–751, 2014.

[98] A. Cohen, R. DeVore, and C. Schwab, "Convergence rates of best n-term galerkin approximations for a class of elliptic spdes," *Foundations of Computational Mathematics*, vol. 10, no. 6, pp. 615–646, 2010.

[99] M. W. Chase Jr and N.-J. T. Tables, "Data reported in nist standard reference database 69, june 2005 release: Nist chemistry webbook," *J. Phys. Chem. Ref. Data, Monograph*, vol. 9, pp. 1–1951, 1998.

Nomenclature

ORC	Organic Rankine Cycle
LNG	Liquefied Natural Gas
NG	Natural Gas
wf	working fluid
T_0	ambient temperature, °C
$\bar{e}$	molar exergy, kJ/kmole
$\bar{h}$	molar enthalpy, kJ/kmole
T	temperature, °C
$\bar{s}$	molar entropy, kJ/K kmole
$\dot{I}$	exergy destruction rate, kJ/h
$\dot{n}$	mole flow rate, kmole/h
$\dot{Q}$	heat transfer rate, kJ/h
M	molar mass, kg
W	power per kilogram LNG, kJ/kmole LNG
η_C	cold exergy efficiency

η_{ex}	exergy efficiency
η_{th}	thermal efficiency
$\bar{W}$	power per kilomole LNG, kJ/hr kgLNG
P	pressure, bar
x	working fluid composition
$\bar{x}$	nomial value of composition
J	objective function
I	uncertainty bound
Y_{pa}	objective function imposed with penalty
Y_{net}	net power output without penalty
s	penalty function
γ	penalty parameter
ΔT_{vi}	violation of reference minimum temperature difference, °C
f_l	lquid fraction of expander outlet
ΔT_{min}	minimum temperature difference, °C
A_h	required heat exchanger area
θ	varied composition
y_α	PCE coefficient
ξ	iso-transformed x
Ψ_α	multivariate PCE basis
ψ	univariage PCE basis

δ	Kronecker delta
$\mathcal{A}$	truncated set of multi-indices
f_ξ	probability density function for ξ
q	level of spars grids
$m(l)$	growth function for one-dimensional quadrature
$\mathcal{U}$	interpolant
d	dimension of uncertainty vector
$\mathcal{A}(q,d)$	Smolyak sparse grid interpolation
Ξ	sparse grids
G	quadrature
z_w	RS model basis
u	design variable
β_w	coefficient for RS model
λ_s	lasso weight

초 록

운전 조건의 변화에 유연한 대처가 가능하며 열역학 파라미터의 측정 오류에 강건한 유기 랭킨 사이클(ORC)을 설계하는 방법론이 개발되었다. 강건한 유기 랭킨 사이클 설계에 앞서, 액화 천연가스(LNG)로부터 최대로 냉열을 추출하기 위해, 다성분 작동 유체를 사용하여 ORC 을 설계하는 방법론이 제안되었다. 제안된 시스템은 다단계의 형태를 보이는 ORC로, 각 단계의 액화기에서 발생하는 엑서지 손실을 최소로 하기 위하여 이 성분 작동 유체를 사용하였다. 각 단계의 작동 유체로서 최적의 혼합물을 찾기 위하여 혼합물의 질량 분율과 압력을 변화시켜 가며 액화기에서 발생하는 엑서지 손질의 최소화를 진행하였다. 최적 작동 유체 혼합물을 선택한 후에 제안된 ORC의 효율 최적화를 위해 ORC 유닛들의 운전 조건들을 이용한 효율 최적화를 시행하였다. 이에 더해 사용된 열원의 온도 변화에 따른 공정 효율의 민감도 분석을 진행하였다.

이어지는 섹션에서는 운전 중 작동 유체의 조성이 변하는 상황에서도 전력을 최대한으로 생산할 수 있는 ORC 설계 방법론이 개발되었다. 제안된 방법은 ORC의 출력이 평균적으로 최대가 되는 설계를 찾는다. ORC의 안정적인 운전에 악영

향을 주는 요소들(열교환기 내의 최소 설계 온도 차 위반과 팽창기 블레이드 표면에 액체방울이 형성)을 억제하기 위해, 이러한 요소들이 발생했을 때 목적 함수가 패널티를 받도록 하였다. 최적화에 필요한 통계학적 모멘트들을 구하는 데에는 두 단계가 필요하다. 우선, 노미날 운전 조건 하에서 ORC 시뮬레이션을 통해 열교환기의 면적을 얻는다. 다음으로 계산된 열교환기 면적을 고정한 상태로 조성을 노미날 값으로부터 변화시켜 다시 시뮬레이션을 진행하고, 이로부터 노미날 운전 조건으로 계산했을 때와는 다른 목적 함수의 값을 얻는다. 조성은 노미날 값을 중심으로 분포되어 있다고 가정하였으며, 이때 조성이 선택될 확률은 모든 범위에서 같다고 가정하였다. ORC 출력의 평균값과 분산값을 적은 수의 샘플들로부터 계산하기 위하여 Polynomial Chaos Expansion(PCE) with sparse grid quadrature가 사용되었다. 최적화를 진행한 결과, 조성의 작은 변화라도 ORC의 안정적인 운전에 심각한 영향을 미칠 수 있다는 사실을 알게 되었으며, 제안된 방법을 통해 조성의 불확실성에도 불구하고 유연한 운전이 가능한 ORC를 설계할 수 있었다.

마지막으로, 조성의 불확실성에 더해 열원의 온도와 열역학 파라미터에도 불확실성이 있는 경우를 위한 최적화 방법이 개발되었다. 이전 섹션에서 조성 변화에 가장 둔감한 것으로 밝혀진 작동 유체를 이용하여, 알려진 임계 온도와 임계 압력에 측정 오차가 있는 경우를 위해 다시 최적화를 진행하였다. 또한, 열원의 온도가 노미날 값에서 벗어나는 경우도 ORC 운전의 유연성을 높이기 위해 고려되었다. 총 9개의 불확실한 열역학 파라미터 혹은 디자인 변수들이 고려되었고, 이는 과도한 계산량을 필요로 하므로 이전 섹션으로 개발된 방법으로는 최적화를 수행하기에 무리가 있었다. 따라서 PCE에 기반한 대체 모델을 이용하여 최적화를 진행하는 방

법이 개발되었다. 개발된 대체 모델은 평균과 분산을 분석적으로(analytically) 구할 수 있게 해주기 때문에 최적화에 걸리는 시간을 급격하게 감소시켜 주었다. 대체 모델을 이용하여 최적화를 진행한 결과 열역학 파라미터의 불확실성과 디자인 조건의 불확실성에도 불구하고 평균적으로 높은 전력을 생산할 수 있는 ORC를 설계하게 되었다.

주요어: 유기 랭킨 사이클, 강건한 설계, Polynomial chaos, 불확실성 정량화, 다성분 작동 유체

학번: 2013-23159